DANISH METEOROLOGICAL INSTITUTE
SCIENTIFIC REPORT
03-14

Long-Term Probabilistic Atmospheric Transport and Deposition Patterns from Nuclear Risk Sites in Euro-Arctic Region

Alexander Mahura[1,2], Alexander Baklanov[1], Jens Havskov Sørensen[1]

[1] Danish Meteorological Institute, Copenhagen, Denmark
[2] Institute of Northern Environmental Problems, Kola Science Centre, Apatity, Russia

Arctic Risk Project of the Nordic Arctic Research Programme (NARP)

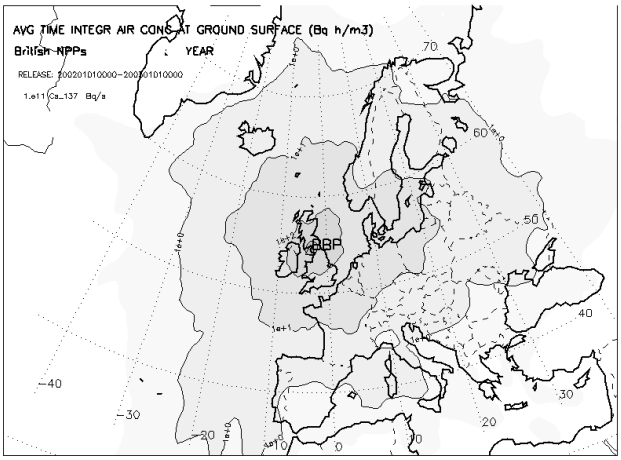

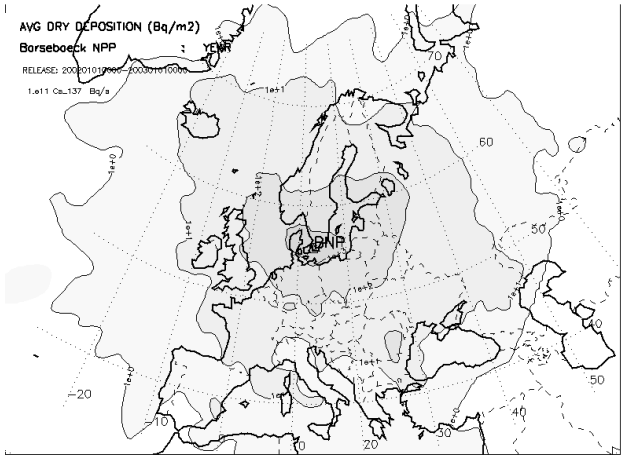

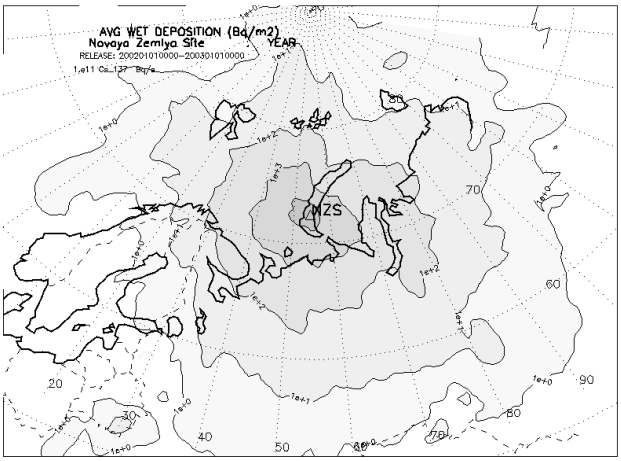

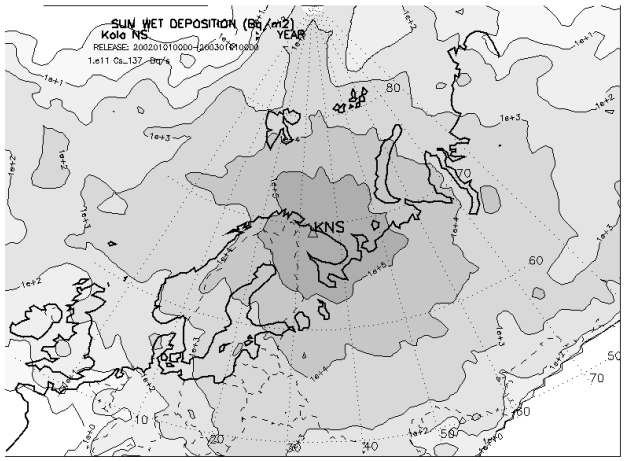

COPENHAGEN 2003

ISSN: 0905-3263 (printed)
ISSN: 1399-1949 (online)
ISBN: 87-7478-490-0

TABLE OF CONTENTS

SUMMARY

The main purpose of the Arctic Risk, NARP multidisciplinary project is to develop a methodology for complex nuclear risk and vulnerability assessment and to test it by estimation of a nuclear risk to population in the Nordic countries in case of a severe accident at nuclear risk sites (NRSs). This report is focused on the testing of the developed methodology (*AR-NARP, 2001-2003; Baklanov et al., 2002b*) and probabilistic evaluation of the long-term atmospheric transport and deposition patterns for radioactive pollutants from selected 16 risk sites in the Euro-Arctic region. The main questions to be addressed are:

What geographical territories and neighbouring countries are at the highest risk of being polluted during atmospheric transport and deposition in case of an hypothetical accident at NRS?

What are levels of contamination on local, regional, and large scales due to dry and wet deposition in case of a hypothetical accident at NRS?

To answer these questions, at first, we applied a combination of DMI's models - 3-D trajectory, DERMA, and HIRLAM. These models were used to simulate a long-term (during year of 2002) atmospheric transport, dispersion, and deposition of ^{137}Cs for a one day hypothetical release (at rate of 10^{11} Bq/s). Then, a set of statistical methods (including exploratory and probability fields analyses) was employed for probabilistic analysis of dispersion modelling results in order to evaluate variability of annual, seasonal, and monthly NRS possible impact indicators, such as average and summary time integrated air concentration (TIAC), dry deposition (DD) and wet deposition (WD) fields.

Among 16 NRSs several groups can be identified based on spatial and temporal variability of calculated fields: sites located in the maritime, continental, arctic, and intermediate (maritime vs. continental) areas. For most of NRSs the prevailing atmospheric transport is by westerlies. The TIAC and DD fields have an elliptical shape compared with more cellular structure of the WD field which strongly depends on irregularity of the rainfall patterns. Moreover, the WD fields can have several local maxima remotely situated from the sites. The ranking of potential impact on Copenhagen, Denmark from selected 16 NRSs of the Euro-Arctic region showed that although for TIAC and DD the order of such ranking is identical; when additionally a wet deposition is accounted the ranks can change significantly already on mesoscales. Due to a relative proximity ($\leq$ 500 km) to Copenhagen, the Barsebaeck, block of the German nuclear power plants (NPPs), Oskarshamn, and Ringhals NPPs represent the risk sites of major concern for the city. Although several other sites such as the Olkiluoto, Ignalina, Loviisa, and Forshmark plants are located geographically closer to the city, the block of the British NPPs ($>$ 1000 km) represents the higher risk of airborne transport potential impact on Copenhagen compared with them.

The results of this study are applicable for: (i) better understanding of general atmospheric transport patterns in the event of an accidental release at NRS, (ii) improvement of planning in emergency response to radionuclide releases from the NRS locations, (iii) studies of social and economical consequences of the NRS impact on population and environment of the neighbouring countries, (iv) multidisciplinary risk evaluation and vulnerability analysis, (v) probabilistic assessment of radionuclide regional and long-range transport patterns, and (vi) evaluation of integrated impact from the long-term releases/ emissions.

The annual, seasonal, and monthly variability of the time integrated air concentration, dry, and wet deposition fields are stored on CD (enclosed with this report with enlarged figures, if ordered).

I. INTRODUCTION

Many international research projects have realized models and methods describing separate parts in evaluation of the risk assessment, e.g. the probabilistic safety assessment, long-range transport and contamination modelling, radioecological sensitivity, dose estimation, etc. However, methodologies for multidisciplinary studies of nuclear risk assessments and mapping are not well developed yet (cf. e.g. *Baklanov, 2002*). As shown in *IIASA, 1996*, the risk-assessment strategy can be realised by the following methods: inference from actual events (i.e. using published results from real events); physical modelling (i.e. using known input and prevalent levels); and theoretical modelling (i.e. using simulated response to assumed scenarios of releases). Description and results of these methods with respect to nuclear risk sites are shown by *IIASA, 1996*; *Moberg, 1991; Bergman et al., 1998; Dahlgaard, 1994; Bergman & Ulvsand, 1994*; *Amosov et al., 1995; Rantalainen, 1995*.

For probabilistic analysis some authors performed studies based on combination of different factors and probabilities. Previous research in the Arctic latitudes were based on employing of the trajectory modelling approach to evaluate potential impact from nuclear plants such as Kola (*Saltbonis, ; Baklanov et al., 2002a*) and Bilibino (*Mahura et al., 1999*). The dispersion modelling approach was used by *Slaper et al., 1994* whom evaluated dispersion of the radioactive plume by a simple model (based on only meteorological station) in order to estimate risks, health effects, and countermeasures due to severe accidents at the European NPPs (including the northern latitudes plants) and a submarine (*NATO, 1998*). *Sinyak, 1995* used some empirical factors to describe the influences of geography resulting in normalized damage factors for the main European cities. *Andreev et al.*, *1998; 2000* simulated dispersion and deposition with a Lagrangian particle model and calculated the frequency of exceedance of certain thresholds for ^{137}Cs, regarded as a risk indicator.

The dispersion and deposition models can be successfully used for separate case studies for typical or worst-case scenarios. They can be used also for probabilistic risk mapping as a more expensive, but alternative of the trajectory analysis methods discussed for the nuclear risk sites by *Baklanov & Mahura, 2001; Mahura & Baklanov, 2002*. Applicability and examples of different models for accidental release dispersion and deposition simulation on the local and regional scales in the Arctic were discussed by *Baklanov et al., 1994; Thaning & Baklanov, 1997; Baklanov, 2000; Baklanov et al., 2001; Baklanov & Sørensen, 2001*).

The methodology, developed in the bounds of the Arctic Risk project (*AR-NARP, 2001-2003*) is a logical continuation, as mentioned by *Baklanov et al., 2002b*, of several previous studies realised in the frameworks of international projects. It includes several specific approaches in optimal strategy of the multidisciplinary methodology. Among these approaches is a combination of the probabilistic analysis and case studies analysis.

In previous AR-NARP project reports (*Baklanov & Mahura, 2001; Mahura & Baklanov, 2002; Baklanov et al., 2002b*) we described a methodology of trajectory and dispersion modelling approaches, methodology results of probabilistic analysis of atmospheric transport pattern and risk assessment based on trajectory modelling. The main purpose of this report is to test and employ the developed methodology (e.g. *AR-NARP, 2001-2003; Baklanov et al., 2002b*) based on a long-term dispersion modelling approach in order to evaluate temporal and spatial variability of atmospheric transport and deposition patterns from sixteen nuclear risk sites in the Euro-Arctic region, and use these patterns for further integration in GIS for risk and vulnerability mapping.

II. SELECTED APPAROACHES

2.1. *NUCLEAR RISK SITES OF INTEREST*

All selected NRSs are located within the area of interest of the "Arctic Risk" Project. These NRSs are represented mostly by the nuclear power plants (NPPs) in Russia, Lithuania, Germany, United Kingdom, Finland, Ukraine, and Sweden (see Tab. 2.1.1, Fig. 2.1.1). It should be noted that the Kola NPP (KNP, Murmansk Region, Russia) has the old type of reactors (VVER-230); Leningrad (LNP, Leningrad Region, Russia), Chernobyl (CNP, Ukraine), and Ignalina (INP, Lithuania) NPPs have the most dangerous RBMK-type reactor. Moreover, the Novaya Zemlya (NZS, Novaya Zemlya Archipelago, and Russia) was considered as the former nuclear weapon test site and potential site for nuclear waste deposit; and the Roslyakovo shipyard (KNS, Murmansk Region, Russia) was considered as a risk site with nuclear power ships in operation or waiting to be decommissioned.

Table 2.1.1. Nuclear risk sites selected for the "Arctic Risk" Project.

#	*Site*	*Lat,°N*	*Lon,°E*	*Site Names*	*Country*
1	***KNP***	67.75	32.75	Kola NPP	Russia
2	***LNP***	59.90	29.00	Leningrad NPP	Russia
3	***NZS***	72.50	54.50	Novaya Zemlya Test Site	Russia
4	***INP***	55.50	26.00	Ignalina NPP	Lithuania
5	***BBP***	54.50	-3.50°W	Block of the British NPPs	United Kingdom
6	***BGP***	53.50	9.00	Block of the German NPPs	Germany
7	***LRS***	60.50	26.50	Loviisa NPP	Finland
8	***TRS***	61.50	21.50	Olkiluoto (TVO) NPP	Finland
9	***ONP***	57.25	16.50	Oskarshamn NPP	Sweden
10	***RNP***	57.75	12.00	Ringhals NPP	Sweden
11	***BNP***	55.75	13.00	Barsebaeck NPP	Sweden
12	***FNP***	60.40	18.25	Forshmark NPP	Sweden
13	***KRS***	51.70	35.70	Kursk NPP	Russia
14	***SNP***	54.80	32.00	Smolensk NPP	Russia
15	***CNP***	51.30	30.25	Chernobyl NPP	Ukraine
16	***KNS***	69.20	33.40	Roslyakovo Shipyard	Russia

The Block of the British NPPs (BBP) is represented by a group of the risk sites: the Sellafield reprocessing plant, Chapelcross (Annan, Dumfriesshire), Calder Hall (Seascale, Cumbria), Heysham (Heysham, Lancashire), and Hunterston (Ayrshire, Strathclyde) NPPs. The Block of the German NPPs (BGP) is represented by a group of NPPs: Stade (Stade, Niedersachsen), Kruemmel (Geesthacht, Schleswig-Holstein), Brunsbuettel (Brunsbuettel, Schleswig-Holstein), Brokdorf (Brokdorf, Schleswig-Holstein), and Unterweser (Rodenkirchen, Niedersachsen). Although these NPPs use different reactor types and, hence, could have different risks of accidental releases, the grouping is relevant for airborne transport studies because all NPPs are located geographically close to each other and, hence, atmospheric transport patterns will be relatively similar. The further evaluation of risk levels can be calculated for each NPP separately based on the atmospheric transport fields and probabilities of accidents for each NPP.

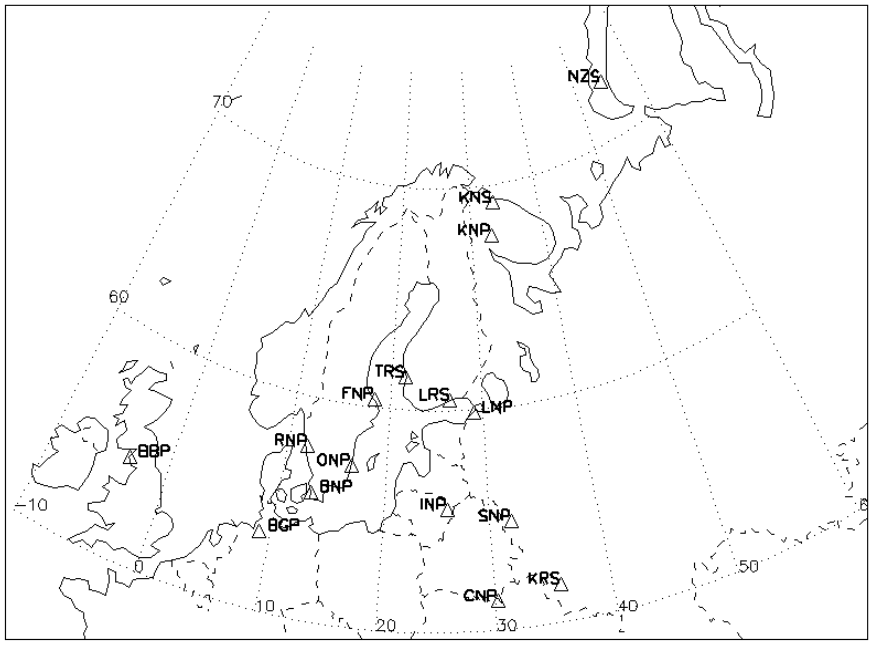

Figure 2.1.1. Selected nuclear risk sites of interest.

2.2. *INPUT METEOROLOGICAL DATA*

In our study, we used two types of the gridded datasets, as input data, for the dispersion modelling purposes. They are the DMI-**HIRLAM** (**HI**gh **R**esolution **L**imited **A**rea **M**odel) and **ECMWF** (**E**uropean **C**entre for **M**edium-Range **W**eather **F**orecast) datasets. The detailed description of these gridded datasets is given by *Baklanov et al. (2002).*

The DMI-HIRLAM dataset was used to model atmospheric transport, dispersion, and deposition only of ^{137}Cs for 16 NRSs during Fall 2001 - Spring 2003 (and will continue through the year of 2003 to obtain further the inter-annual variability of calculated parameters and longer multiyear statistics which is more representative compared with a short-term modelling). The ECMWF dataset (domain covers nearly the entire Northern Hemisphere, i.e. extends between 12˚N–90˚N vs. 180˚W–180˚E) was used to model atmospheric transport, dispersion, and deposition for three radionuclides - ^{137}Cs, ^{131}I, and ^{90}Sr – but only from one NRS (Leningrad NPP).

The model runs based on different types of datasets were performed for comparison purposes, and first of all, to compare the accuracy of the wet deposition patterns. For the specific case studies, both datasets were used.

2.3. *LONG-TERM DISPERSION MODELLING USING DERMA*

In this study, we used the **D**anish **E**mergency **R**esponse **M**odel for **A**tmosphere (**DERMA**), developed by DMI for nuclear emergency preparedness purposes, which is a numerical 3-D atmospheric model of the Lagrangian type. DERMA was used to simulate a long-term (during year of 2002) atmospheric transport, dispersion, and deposition of radionuclide from the selected NRSs. It considered also processes of radioactive decay and removal by precipitation during atmospheric transport. As input meteorological data, DERMA uses: 1) the **N**umerical **W**eather **P**rediction (**NWP**) model data from different operational versions of the HIRLAM or 2) global model of the **E**uropean **C**entre for **M**edium-Range **W**eather **F**orecast (**ECMWF**) model data. The detailed

description of the DERMA model is given by *Sørensen, 1998*; *Sørensen et al., 1998*; *Baklanov & Sørensen, 2001; Baklanov et al., 2002b* and used in this study assumptions by *Baklanov et al., 2002b.*

It should be repeated again that the following characteristics (for a daily continuous **d**iscrete **u**nit **h**ypothetical **r**elease (DUHR) of ^{137}Cs at NRSs at rate of 10^{11} Bq/s) were calculated: 1) air concentration (Bq/m^3) in the surface layer; 2) time-integrated air concentration (Bq·h/m^3); 3) dry and wet deposition (Bq/m^2) fields. These fields were recalculated in a gridded domain of a resolution of 0.5˚ vs. 0.5˚ of latitude vs. longitude, shown in Fig. 2.3.1 (30-89˚N vs. 60˚W-135˚E). Moreover, these fields are limited during one year by consideration of 5 days of atmospheric transport of radioactive matter after release ended.

The SGI Origin scalar server was used for DERMA runs and the NEC SX6 supercomputer system of DMI was used for DMI-HIRLAM modelling computational purposes. All modelled data were stored on the DMI UniTree mass-storage device as well as recorded on CDs.

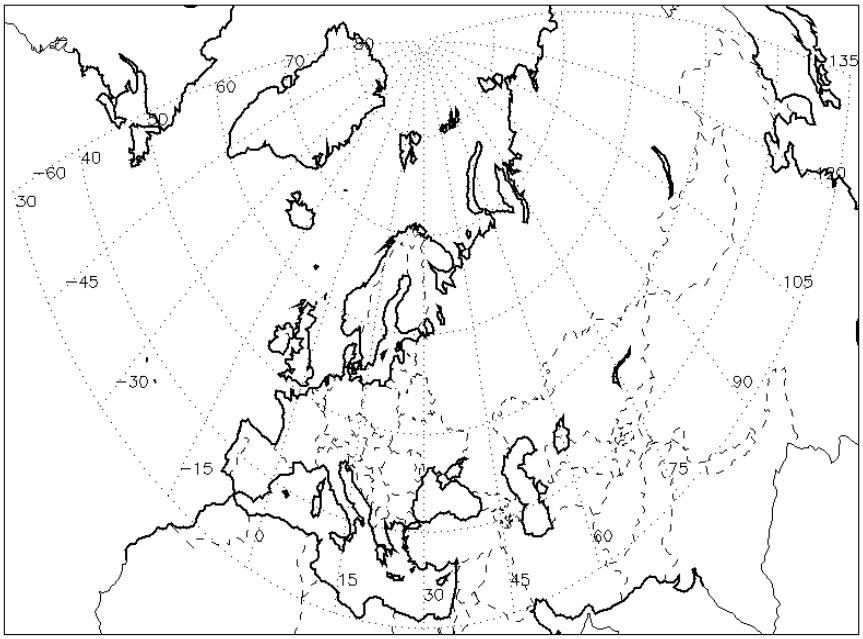

Figure 2.3.1. Domain of recalculated dispersion modelling fields.

2.4. *INDICATORS OF NRS IMPACT BASED ON DISPERSION MODELLING RESULTS*

Two approaches were selected to construct fields for calculated characteristics during the time period of interest (for instance: month, season, or year). The first type – summary field – is based on calculating the distribution of the total sum of daily DUHR of radioactivity at NRS during the period considered, and note that it is a field integrated over this period. This type of field shows the most probable geographical distribution of radionuclide when the release of radioactivity occurred during the entire period considered. The second type – average field – is based on calculating the average value from the summary field. This type of field shows the most probable geographical distribution of radionuclide when the release of radioactivity occurred during one average day within the period considered.

In this report we presented only the time integrated air concentration (TIAC), dry deposition (DD), and wet deposition (WD) patterns from all potential indicators of the NRS impact (shown in Fig. 2.4.1) on selected geographical regions and territories, and countries of concern (shown in Fig. 2.4.2). The total deposition (TD) fields can be simply calculated by summing of the dry and wet

depositions. Only one year (January-December 2002) of calculated fields was used to construct the NRS impact indicators. For convenience of comparison the temporal variability in characteristic patterns was underlined by isolines at similar intervals, although every field can be easily reconstructed with different threshold orders of magnitude than selected. It should be noted that although these fields were calculated for DUHR, it is possible to recalculate or rescale them for another accidental release of radioactivity at different magnitude rates. Other assumptions used in this study are discussed by *Baklanov et al., 2002b.*

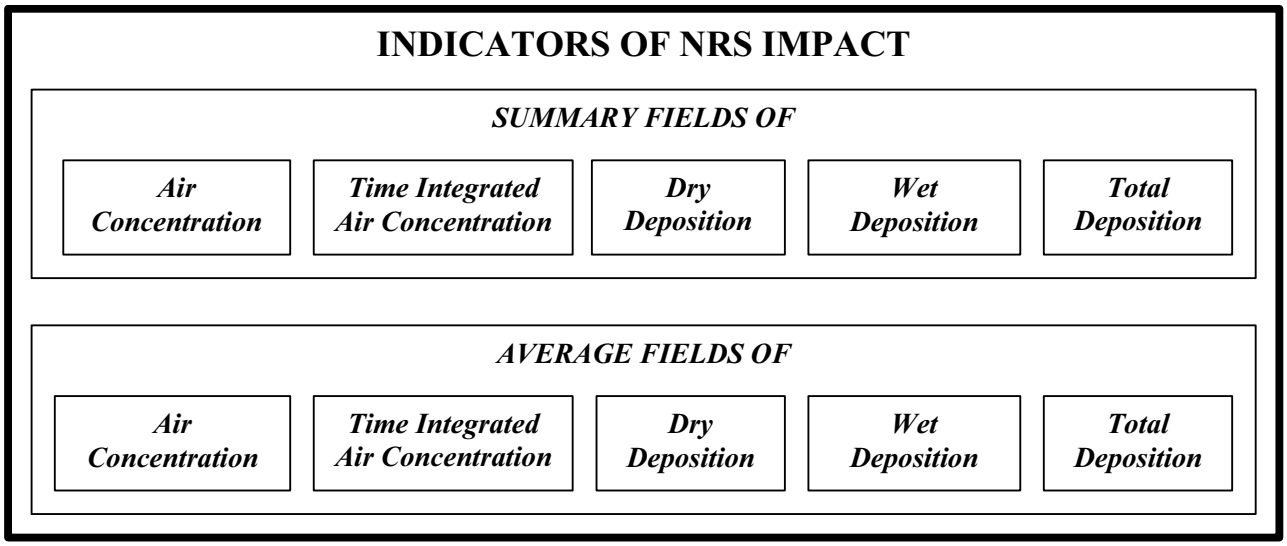

Figure 2.4.1. Indicators of nuclear risk site impact based on dispersion modelling results.

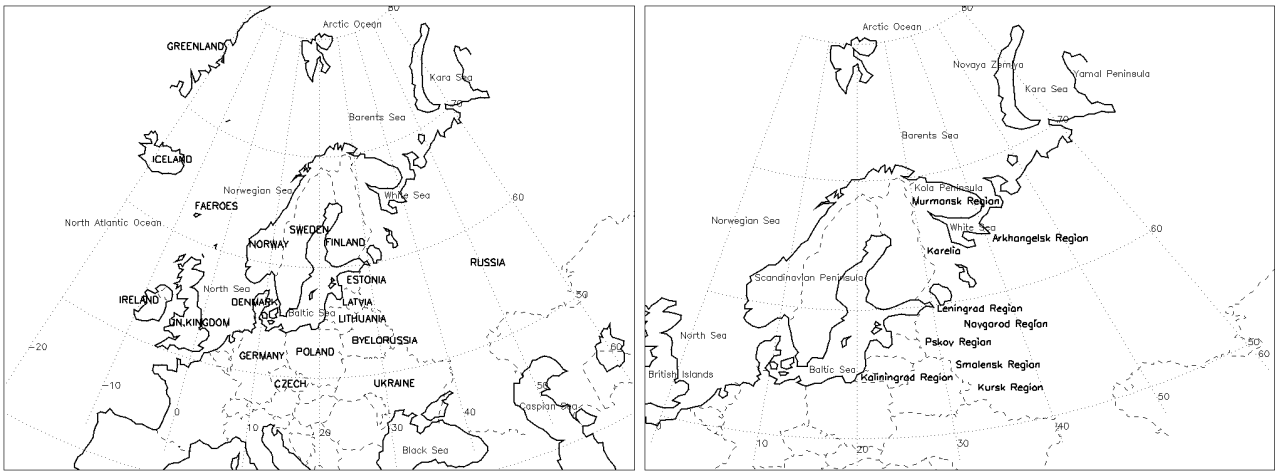

Figure 2.4.2. Geographical regions, territories, and countries selected for the "Arctic Risk".

III. ASSESSMENT OF ATMOSPHERIC DISPERSION MODELLING RESULTS FROM NUCLEAR RISK SITES IN EURO-ARCTIC REGION

In this chapter, we will focus on evaluation of the long-term dispersion modelling results (based on modelling of 5 days atmospheric transport after the hypothetical releases completed at the sites) which are represented as indicators of the NRS impact. Moreover, we will consider several specific case studies. Using such indicators (based on dispersion modelling results) of the NRS impact we plan further to employ different dose calculation models as well as the GIS-based risk and vulnerability analysis for population and environment, first of all, of the Nordic countries.

In this study we calculated and constructed two categories of fields - summary and average – for ^{137}Cs time integrated air concentration (TIAC), dry deposition (DD), and wet deposition (WD) patterns. In this chapter, we will consider only the annual average fields, although the summary fields are stored on CD (enclosed with this report with enlarged figures, if ordered). The scaling with similar magnitude isolines starting from the lowest of 10^{+2} (1e+2 in figures) is used to simplify interpretation and comparison of fields, although other scale can be selected and fields re-plotted based on the original archived data. Additionally, an estimation of the TIAC, DD, WD, and TD patterns resulted from atmospheric accidental releases at several NRSs was performed for selected European cities shown in Tab. 3.1 (*the Nordic countries with capitals are given in Italic style of format*).

Table 3.1. Selected geographical locations/cites by countries.

City, Country	***Latitude, N***	***Longitude, E***	***City, Country***	***Latitude, N***	***Longitude, E***
Copenhagen, Denmark	55.67	12.58	Kiev, Ukraine	50.43	30.52
Helsinki, Finland	60.60	21.43	Bucharest, Romania	44.43	26.10
Oslo, Norway	59.92	10.75	Warszawa, Poland	52.25	21.00
Stockholm, Sweden	59.33	18.05	Praha, Czech Republic	50.08	14.47
Reykjavik, Iceland	64.15	-21.95W	Bratislava, Slovakia	48.15	17.12
Torshavn, Faeroes	62.03	-6.78W	Luxembourg, Luxembourg	49.61	6.13
Nuuk, Greenland	64.25	-51.58W	Amsterdam, Netherlands	52.35	4.92
St.Petersburg, Russia	59.89	30.26	Minsk, Belarus	53.90	27.57
Moscow, Russia	55.75	37.58	Dublin, Ireland	53.33	-6.250W
Vienna, Austria	48.20	16.37	Bern, Switzerland	46.92	7.47
Paris, France	48.87	2.33	Tallinn, Estonia	59.43	24.73
London, UK	51.52	-0.11W	Riga, Latvia	56.95	24.10
Brussels, Belgium	50.83	4.33	Vilnius, Lithuania	54.67	25.32
Berlin, Germany	52.52	13.40	Budapest, Hungary	47.50	19.08

Some important comments should also be taken into account. First, it should be noted that using average and summary fields it is possible to interpolate data to a particular geographical area of interest (enclosed by geographical boundaries) or for a particular geographical location (for example, a city). Second, the summary fields can be used further to calculate doses accumulated over a considered period (month, season, year) – i.e. monthly doses, seasonal doses, or annual doses. These summary fields will be more representative if the routine discharges of radioactivity from NRS are considered. Third, the average fields will be used further to calculate doses accumulated from a one day hypothetical release averaging over a considered period (month, season, and year) – i.e. average daily doses for a particular month, season, or year. These average fields will be more representative if the accidental short-term releases of radioactivity from NRS are investigated. Fourth, the summary fields will have larger areas enclosed by isolines, and magnitudes of TIAC, DD, and WD will be higher compared with the average fields. Fifth, because all fields

were calculated for the discrete unit hypothetical release (DUHR), it is possible to recalculate or rescale these fields for other accidental release of radioactivity at different magnitude rates. Sixth, in calculating atmospheric transport and deposition of radioactivity releases (with a duration of one day) at NRSs, we limited our calculation to 5 days after the release was completed at the site. As uncertainties in modelling of atmospheric transport after 5 days became too great, for the calculated fields of one-day releases we did not apply any loss processes after that 5 day term. It might be that after this term the trajectories still did not leave the model grid domain and following the mass conservation law these trajectories will provide additional contributions into concentration and deposition fields. But, we assume, that mostly trajectories will leave the selected domain with regions of interest in our study (shown in Fig. 2.3.1) and contributions at boundaries of the calculated fields will be significantly smaller, is the average fields are considered. Moreover, once material was deposited on the surface, the radioactive decay was not considered, although it should be accounted for further risk and vulnerability analyses.

3.1. *TIME INTEGRATED AIR CONCENTRATION PATTERNS FOR ^{137}CS*

The time integrated air concentration (TIAC) of a radionuclide is input data to calculate doses due to inhalation. It is an air concentration of radionuclides accumulated during a selected time interval. Therefore, for example, for a particular month, the average monthly field might be used to calculate an average dose due to inhalation at any selected geographical location at any given day of a particular month. The summary monthly field might be used to calculate the monthly dose due to inhalation at any selected geographical location.

Let us mention some common peculiarities. First, the time integrated air concentration fields have a distribution type of isolines around the site, which is closer to elliptical than circular. The shape of these fields, in some way, reflects the presence of dominating airflow patterns throughout the year. These airflow patterns could be also obtained from the results of trajectory modelling, cluster analysis, and probability fields analysis of 5-day trajectories given by *Mahura & Baklanov, 2002*. Second, the larger magnitudes of TIAC are observed near the sites, and they decrease significantly with distance, as expected.

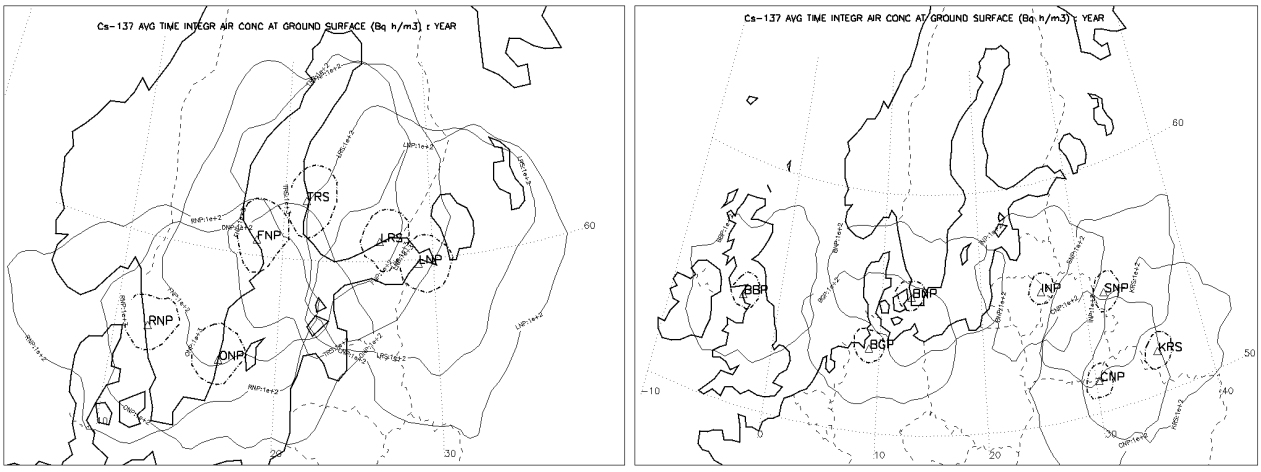

Figure 3.1.1. Annual average ^{137}Cs time integrated air concentration fields for ONP, TRS, LNP, RNP, FNP, LRS (left) and BGP, INP, KRS, BBP, BNP, SNP, CNP (right) risk sites.

The annual average TIAC fields for the risk sites selected in this study are shown in Fig. 3.1.1 – for NRSs located in the North European region, and in Fig. 3.1.2 – for NRSs located in the Arctic region. The seasonal variabilities of the average and summary TIAC fields for all these sites are

shown in Appendixes 1 and 2, and monthly variability - on CD (enclosed with this report with enlarged figures, if ordered). For simplicity of interpretation and comparison two isolines of 1e+2 (or 10^{+2}) and 1e+3 (10^{+3}) Bq·h/m^3 were plotted on figures.

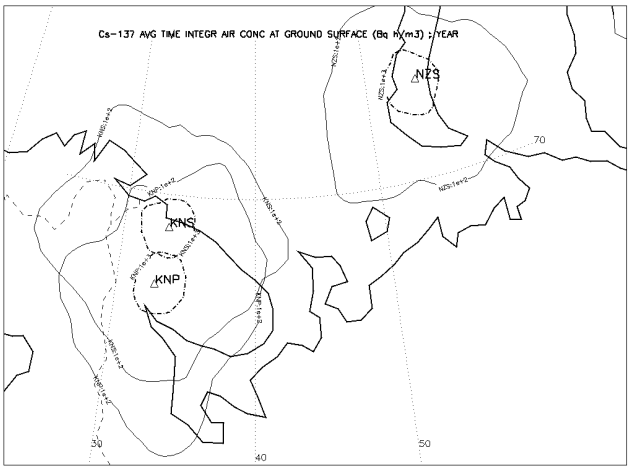

Figure 3.1.2. Annual average ^{137}Cs time integrated air concentration fields for KNS, KNP, and NZS risk sites.

On an annual scale, the highest TIAC (≥1e+3 Bq·h/m^3) are within a first few hundred kilometres around all NRSs. The isolines of 1e+2 Bq·h/m^3 for both Arctic NRSs - NZS and KNS - are more extended in the southern sector from the sites compared to northern sector. For NZS this isoline passes over un-populated areas compared with the KNS and KNP sites. The populated territories of the Kola Peninsula and Karelia as well as northern territories of Norway and Finland are enclosed by isoline of 1e+2 Bq·h/m^3, and they remain more affected by potential accidental releases compared with other territories. Note when only trajectories for the NZS site (see analysis of trajectory modelling results by *Mahura & Baklanov; 2001*) were used to construct the airflow probability fields than the total area of the territories situated under the potential impact from this site was higher compared with other sites. The dispersion approach gave another picture because of including effects of stronger dispersion for the strong wind situations in the Arctic latitudes.

Table 3.1.1. Annual average ^{137}Cs time integrated air concentration at selected European cities resulted from the hypothetical release at the Leningrad NPP.

City, Country	Dist to LNP, km	TIAC, Bq·h/m^3	City, Country	Dist to LNP, km	TIAC, Bq·h/m^3
Minsk, Belarus	**673**	3,73E+1	Budapest, Hungary	1522	1,32E+0
St.Petersburg, Russia	**70**	2,75E+3	Bucharest, Romania	1731	1,39E+0
Moscow, Russia	**686**	4,07E+1	Warszawa, Poland	**983**	8,01E+0
Kiev, Ukraine	**1057**	6,85E+0	Praha, Czech Republic	**1426**	3,13E+0
Stockholm, Sweden	**618**	3,48E+1	Bratislava, Slovakia	1515	1,70E+0
Oslo, Norway	**1014**	8,28E+0	Luxembourg, Luxembourg	1845	1,91E+0
Helsinki, Finland	**424**	5,28E+1	Amsterdam, Netherlands	1699	3,15E+0
Copenhagen, Denmark	**1077**	1,50E+1	*Reykjavik, Iceland*	2625	1,19E-1
Vienna, Austria	1535	1,42E+0	Dublin, Ireland	2246	1,25E-1
Paris, France	2095	1,50E+0	Bern, Switzerland	2012	3,75E-1
London, UK	2025	2,12E+0	Tallinn, Estonia	**245**	1,80E+2
Brussels, Belgium	1840	3,09E+0	Riga, Latvia	**435**	6,36E+1

Torshavn, Faeroes	1920	2,89E-1	*Nuuk, Greenland*	3939	9,58E-6
Berlin, Germany	**1261**	7,99E+0	Vilnius, Lithuania	**622**	4,31E+1

The structure of the concentration field for the BBP site reflects the fact that the most impacted territories are located within boundaries of the British Islands. The potentially affected areas for other sites, except the Kursk and Chernobyl NPPs, are extended within the 50-65°N latitudinal belt. For NRSs of the Scandinavian countries the affected territories are generally parts of the Nordic countries, Baltic States, and border areas of the Northwest Russia. The ^{137}Cs TIACs were estimated at several most populated European cities on example of the annual average TIAC field from the Leningrad NPP (Tab. 3.1.1). At these cities the TIAC decreases by two orders of magnitude within a first 500-km range from the plant. The highest TIAC – 2.75e+3 Bq·h/m^3 - is at St.Petersburg, Russia due to proximity to the nuclear plant. Within the next 500-km range the TIAC values vary between the first and zero orders of magnitudes, after that they drop by an additional order of magnitude reaching a minimum of 3.75e-1 Bq·h/m^3 at Bern, Switzerland. After 2000-km of atmospheric transport from the LNP site the initial TIAC had decreased mostly by three-four orders of magnitude compared with the area closer to the plant. The concentration at the remotest city (Nuuk, Greenland) was even by 9 orders of magnitude smaller – 9.58e-6 Bq·h/m^3.

3.2. *DRY DEPOSITION PATTERNS FOR ^{137}CS*

The dry deposition (DD) of a radionuclide is input data, as important component, to calculate doses from the underlying surface. Dry deposition reflects the concentration of radionuclide deposited at the surface due to the dry deposition process. Doses should include contribution of both – dry and wet – depositions processes, although it is possible to use only dry deposition. In this case, doses would be underestimated because wet deposition is also an important contributor.

Similar to TIAC, for a particular month, the average DD monthly field might be used to calculate an average dose from the underlying surface at any selected geographical location at any given day of a particular month. The summary monthly field might be used to calculate the monthly dose from the underlying surface at any selected geographical location.

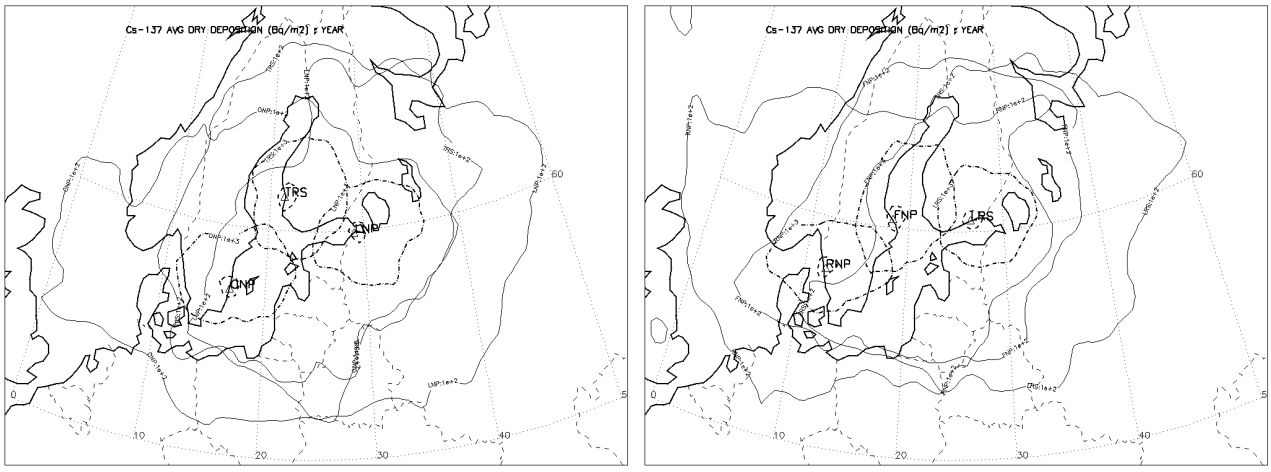

Figure 3.2.1. Annual average ^{137}Cs dry deposition fields for the ONP, TRS, LNP (left) and RNP, FNP, LRS (right) risk sites.

The dry deposition patterns reflect in some way a structure of the time integrated air concentration patterns. Therefore, the elliptical configuration of both fields is similar. The dry deposition reaches its highest values in vicinity of the site. Dry deposition fields are as reliable an

indicator of the prevailing atmospheric transport patterns as an airflow probability field. In particular, for all selected NRSs there is a clear tendency of atmospheric transport by westerly flows.

The annual average DD fields for the risk sites selected in this study are shown in Figs. 3.2.1-3.2.2 – for NRSs located in the North European region, and in Fig. 3.2.3 – for NRSs located in the Arctic region. The seasonal variabilities of the average and summary DD fields for all these sites are shown in Appendixes 1 and 2, and monthly variability - on CD (enclosed with this report with enlarged figures, if ordered). Similarly to TIAC, for simplicity of interpretation and comparison the three isolines of 1e+2 (10^{+2}), 1e+3 (10^{+3}), and 1e+4 (10^{+4}) Bq/m^2 were plotted on figures.

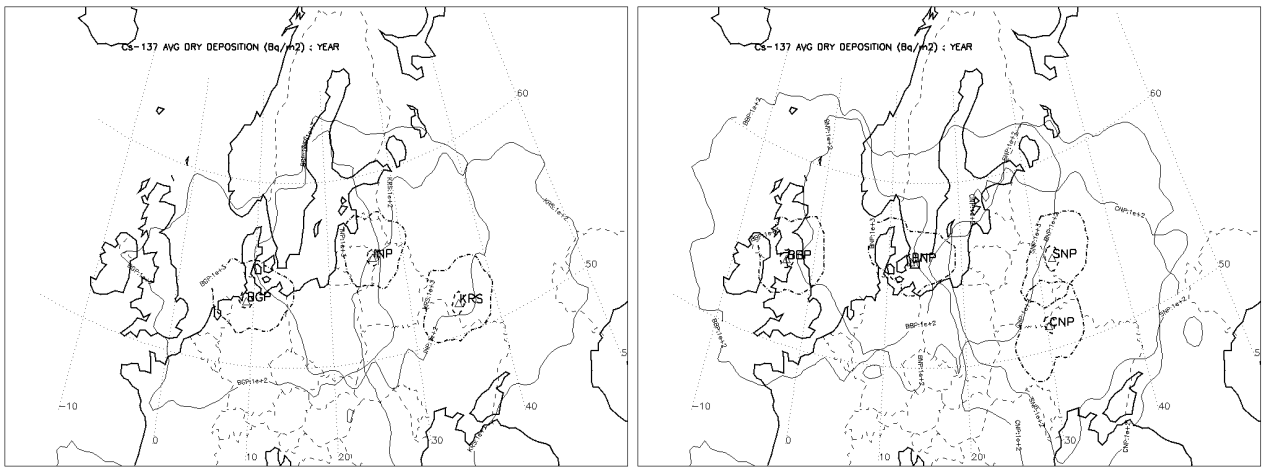

Figure 3.2.2. Annual average ^{137}Cs dry deposition fields for the BGP, INP, KRS (left) and BBP, BNP, SNP, CNP (right) risk sites.

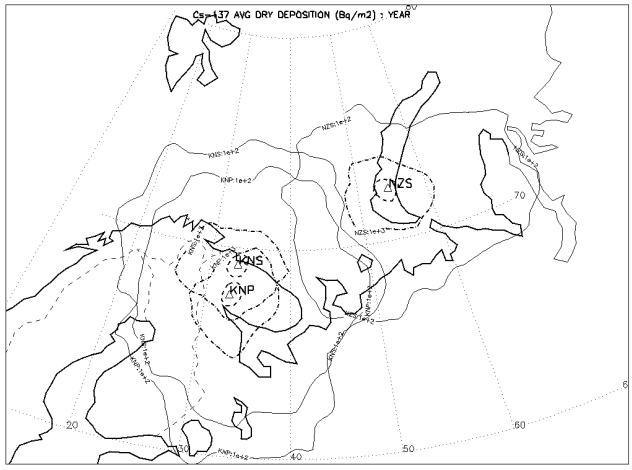

Figure 3.2.3. Annual average ^{137}Cs dry deposition fields for the KNS, KNP, and NZS risk sites.

As seen from all these figures, the highest depositions are in vicinity of the sites. Taking into account isolines of similar magnitude, it should be noted that the DD fields are more extended in the N-S (3-6 degrees) and W-E (5-10 degrees) directions compared with the TIAC fields. For example, considering an isoline of 1e+2 Bq/m^2, for the Arctic NRSs the affected populated areas are extended more to the south and west of the sites and covered large parts of Finland and Northwest Russia. For the NZS site, it is extended more in the western and eastern directions reaching the Kanin and Yamal Peninsulas, respectively. For the British site the DD boundaries extend further to

north and east of the site compared with the same order of magnitude isoline of the TIAC field. For the European sites these boundaries reach as farther south as 50ºN. For the Scandinavian NPPs the isolines reached as farther north as the Kola Peninsula with a significant extension in the eastern direction too. For the KRS, CNP, and SNP plants the DD boundaries almost reach the Black Sea aquatoria. The estimated DD at selected European cities will be discussed in the next section with the wet deposition patterns for comparison of dry and wet deposition contributions into the total deposition pattern.

3.3. *WET DEPOSITION PATTERNS FOR ^{137}CS*

The wet deposition (WD) patterns are different than the time integrated air concentration and dry deposition patterns. The wet deposition fields are less smooth and often have a cellular structure, because they reflect irregularity of the rainfall patterns. It is a concentration of radionuclide deposited at the surface due to removal processes by precipitation or scavenging. The total deposition (TD) is a sum of dry and wet depositions, and it is main input data to calculate doses from the underlying surface and from the nutrition pathways.

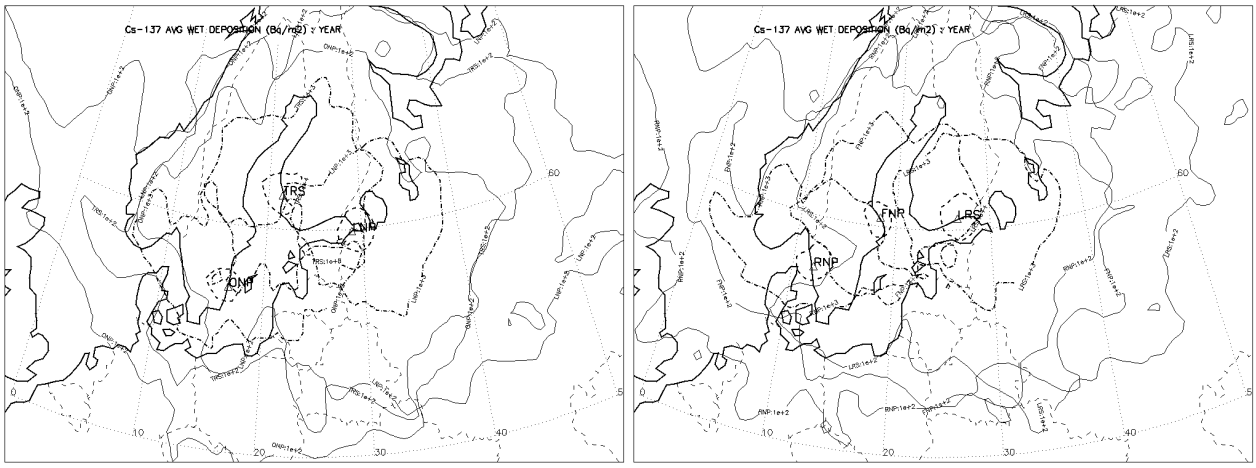

Figure 3.3.1. Annual average ^{137}Cs wet deposition fields for ONP, TRS, LNP (left) and RNP, FNP, LRS (right) risk sites.

The annual average WD fields for the risk sites selected in this study are shown in Figs. 3.3.1-3.3.2 – for NRSs located in the North European region, and in Fig. 3.3.3 – for NRSs located in the Arctic region. The seasonal variabilities of the average and summary WD fields for all these sites are shown in Appendixes 1 and 2, and monthly variability - on CD (enclosed with this report with enlarged figures, if ordered). Similarly to DD, for simplicity of interpretation and comparison the three isolines of 1e+2 (10^{+2}), 1e+3 (10^{+3}), and 1e+4 (10^{+4}) Bq/m^2 were plotted on figures.

As seen from all these figures, the highest wet depositions (1e+4 Bq/m^2) are in vicinity of the sites within a 300-400 km range. Taking into account isolines of similar magnitude, it should be noted that the WD fields are more extended in all directions compared with both TIAC and DD fields. For example, considering an isoline of 1e+2 Bq/m^2, for the Arctic NRSs the affected populated areas are extended farther more to the south and west of the sites covering the northern parts of Norway, Sweden, most of Finland, and Northwest Russia (southerly of 60°N). For the NZS site it is extended even farther to the east (easterly of 70°E) of the site, and reaches Kola Peninsula territories. For the British site the WD field boundaries extend further in the NW-NE sector reaching populated Iceland at north and the Scandinavian and inland European countries at east. For the European risk sites these boundaries reach as farther as southerly of 50ºN and as farther as

easterly of 40ºE. For the Scandinavian NPPs the isolines reached as farther north as the Barents Sea with a significant extension in the eastern direction passing through the 50ºE longitude. For the KRS, CNP, and SNP plants the WD boundaries passed over the Black Sea aquatoria and almost reached the Caspian Sea.

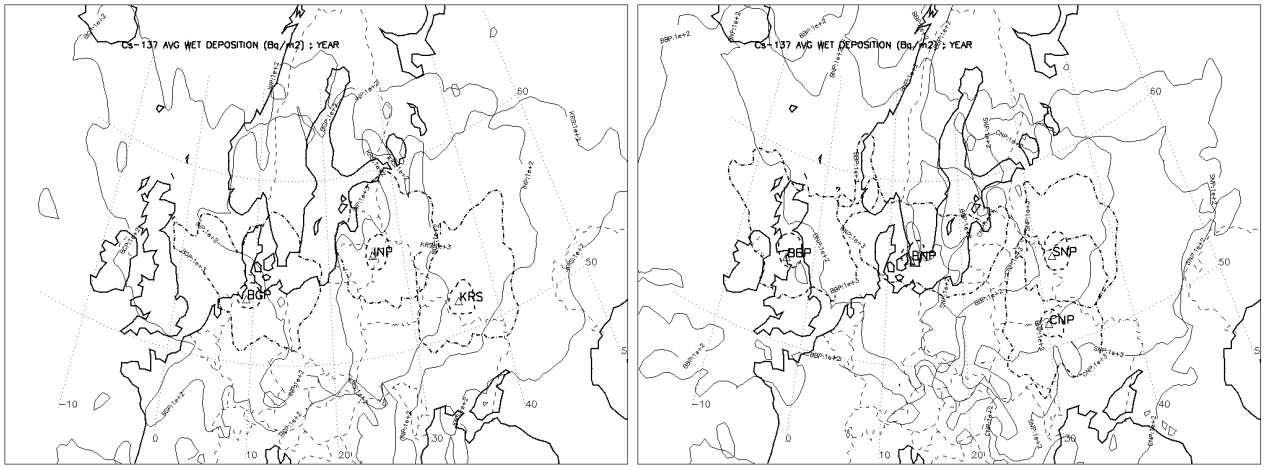

Figure 3.3.2. Annual average ^{137}Cs wet deposition fields for BGP, INP, KRS (left) and BBP, BNP, SNP, CNP (right) risk sites.

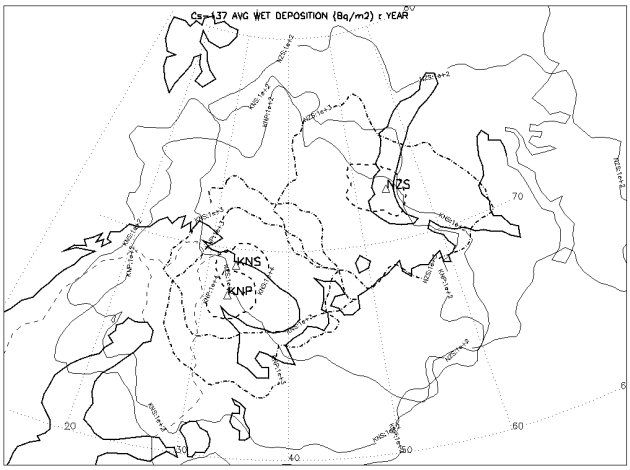

Figure 3.3.3. Annual average ^{137}Cs wet deposition fields for KNS, KNP, and NZS risk sites.

Table 3.3.1. Annual average ^{137}Cs dry, wet, and total depositions, and contribution of both dry and wet depositions into total deposition at selected European cities resulted from the hypothetical release at the Leningrad NPP.

City, Country	Dist to LNP, km	DD, Bq/m^2	WD, Bq/m^2	TD, Bq/m^2	DD/TD, %	WD/TD, %
Minsk, Belarus	673	2,01E+2	1,81E+2	3,83E+2	53	47
St.Petersburg, Russia	70	1,48E+4	3,45E+4	4,93E+4	30	70
Moscow, Russia	686	2,20E+2	4,75E+2	6,94E+2	32	68
Kiev, Ukraine	1057	3,70E+1	7,23E+1	1,09E+2	34	66
Stockholm, Sweden	618	1,88E+2	1,60E+2	3,48E+2	54	46
Oslo, Norway	1014	4,47E+1	1,60E+2	2,04E+2	22	78
Helsinki, Finland	424	2,85E+2	7,51E+2	1,04E+3	28	72

Copenhagen, Denmark	**1077**	8,10E+1	7,68E+1	1,58E+2	51	49
Vienna, Austria	1535	7,66E+0	1,43E+1	2,19E+1	35	**65**
Paris, France	2095	8,07E+0	3,20E+0	1,13E+1	72	28
London, UK	2025	1,14E+1	9,14E+0	2,06E+1	56	44
Brussels, Belgium	1840	1,67E+1	6,77E+0	2,35E+1	71	29
Berlin, Germany	**1261**	4,31E+1	5,21E+1	9,53E+1	45	**55**
Budapest, Hungary	1522	7,10E+0	4,26E+0	1,14E+1	62	38
Bucharest, Romania	1731	7,53E+0	4,07E+0	1,16E+1	65	35
Warszawa, Poland	**983**	4,32E+1	2,38E+1	6,71E+1	64	36
Praha, Czech Republic	**1426**	1,69E+1	2,75E+1	4,44E+1	38	**62**
Bratislava, Slovakia	1515	9,16E+0	1,37E+1	2,29E+1	40	**60**
Luxembourg, Luxembourg	1845	1,03E+1	4,08E+0	1,44E+1	72	28
Amsterdam, Netherlands	1699	1,70E+1	6,56E+0	2,36E+1	72	28
Reykjavik, Iceland	2625	6,43E-1	5,95E-1	1,24E+0	52	48
Dublin, Ireland	2246	6,73E-1	2,00E+0	2,67E+0	25	**75**
Bern, Switzerland	2012	2,03E+0	1,19E+1	1,39E+1	15	**85**
Tallinn, Estonia	**245**	9,70E+2	1,14E+3	2,11E+3	46	**54**
Riga, Latvia	**435**	3,43E+2	3,11E+2	6,54E+2	52	48
Vilnius, Lithuania	**622**	2,33E+2	1,52E+2	3,85E+2	61	39
Torshavn, Faeroes	1920	1,56E+0	1,39E+0	2,96E+0	61	39
Nuuk, Greenland	3939	5,17E-5	3,89E-5	9,06E-5	53	47

As shown in Tab. 3.3.1, on example of a hypothetical release from the Leningrad NPP, the contribution of wet deposition vs. dry deposition into the total deposition vary significantly from city to city. Among all considered capitals, 9 cities showed approximately equal contribution of both depositions - 50±5%. The WD contribution is more than 70% of TD for another 8 cities selected in this study. The DD contribution is more than 70% of TD for another 4 cities (i.e. twice less than for WD), which are the Benelux countries and France and which are located farther west from the LNP site. We should note that there is a peculiarity: at larger distances (more than 1000-km) from the site the contribution of WD became greater.

3.4. *GENERAL STATISTICS AND CORRELATIONS BETWEEN PATTERNS*

In statistical analysis, if concentration of pollutants differing by orders of magnitude is investigated than use of log-transformation for original data is considered as an important step. Hence, all calculated ^{137}Cs TIAC, DD, and WD fields were initially log-transformed, and then subsequent statistics was obtained. Let us consider descriptive statistics on example of the Leningrad NPP.

Table 3.4.1. Descriptive statistics for the log-transformed annual average ^{137}Cs time integrated air concentration, dry, and wet deposition fields for the Leningrad NPP.

Field	Range	Min	Max	Mean	Std. Dev	Variance	Skewness	Kurtosis
Log10_TIAC	12,60	-6,00	6,60	0,88±0.01	2,33	5,41	-0,45±0.01	-0,34±0.03
Log10_DD	13,34	-6,00	7,34	1,57±0.01	2,38	5,65	-0,53±0.01	-0,12±0.03
Log10_WD	13,67	-6,00	7,67	1,79±0.01	2,39	5,71	-0,59±0.01	-0,03±0.03

A set of descriptive statistics - including range, variance, standard deviation, minimum and maximum, and mean, skewness and kurtosis with a standard error - was calculated (Tab. 3.4.1). As shown in Fig. 3.4.1, the given distribution histograms of log-transformed data for all fields have the skewed (in the section of the lower values – to the left) nature. The vertical axis represents the number of the cases when level of such concentration and depositions were observed. The

horizontal axis represents the log-transformed values of concentration – Log10_TIAC (in Bq·h/m^3) and depositions – Log10_DD and Log10_WD (in Bq/m^2). As seen also from the table all characteristics are higher for the wet deposition patterns compared with two others.

The correlations were estimated between TIAC, DD, and WD fields (Fig. 3.4.2). The best fit of data was presented by the linear regression lines. All fields showed a statistically significant (applying the 2-tailed test) strong positive correlation (with $R^2 \approx 0.972$-0.999). The correlation between TIAC and DD was higher ($R \approx 0.999$) compared with correlation of these both with WD ($R \approx 0.986$). Such strong correlation between TIAC and DD also depend on, first of all, the deposition parameterization scheme (employed in this version of the DERMA model), which uses a limited number of the land-use categories.

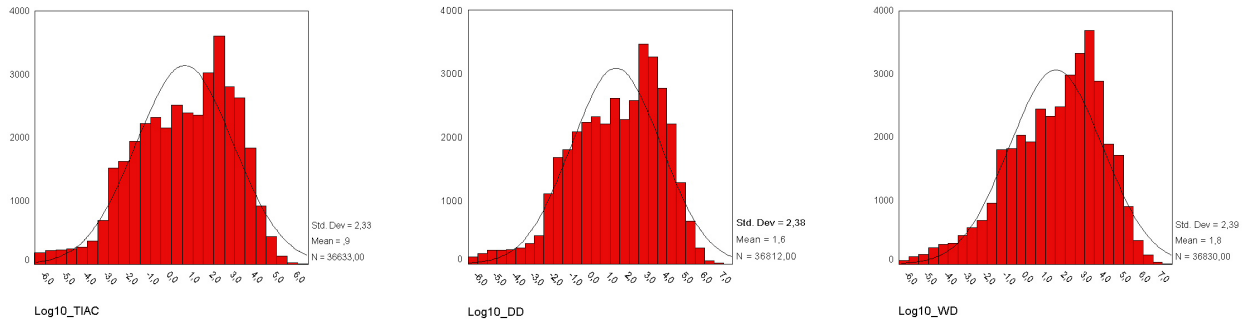

(a) (b) (c)

Figure 3.4.1. Histograms of distribution of the log-transformed annual average ^{137}Cs (horizontal axis – magnitude, vs. vertical axis - # of cases) for a) time integrated air concentration, b) dry deposition, and c) wet deposition fields for the Leningrad NPP.

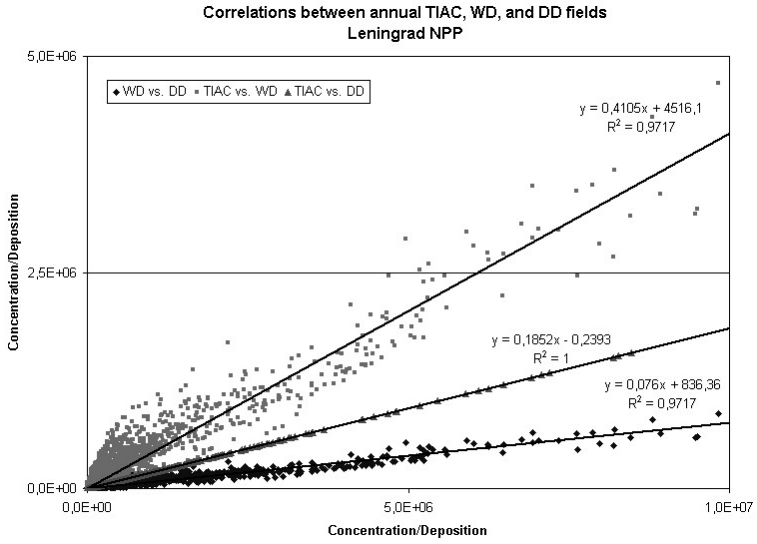

Figure 3.4.2. Correlation between annual average ^{137}Cs time integrated air concentration, dry, and wet deposition fields.

Moreover, the concentration and depositions were evaluated as a function of a radial distance from the Leningrad NPP as shown in Fig. 3.4.3. These were also evaluated using a box-plot procedure with a division on seven distance classes (from 0 to 6 as shown on legend of Fig. 3.4.4). The highest concentration and depositions are generally occurred within a first 1000-km range from the LNP site with a low variability of one-two orders of magnitude. After 1500-km the range of their variability became larger – within several (6-10) orders of magnitude, although the mean

decreased normally following the radioactive decay. The gap between classes 4 and 6, as seen on figures and box-plots, shows differences in airflow patterns from the site. In particular, the higher concentrations are more often observed to the south of the risk site (southerly of the LNP latitude – 59.90ºN) than to the north of the site, but after 4000km they became comparable. Similarly, it is for the east (westerly of 29.0°E) compared with the west. It is important to say here that we focused on the regional scale of the Northern Europe, and therefore, we limited our region of interest up to 4000-km from the site.

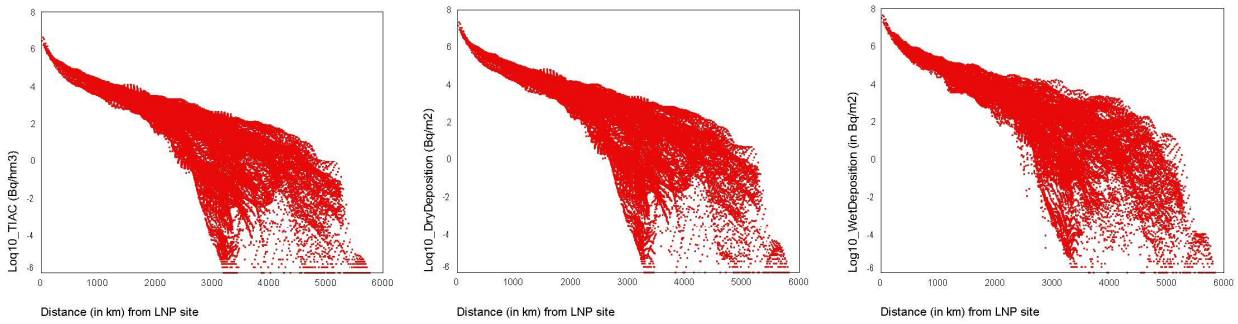

(a) (b) (c)

Figure 3.4.3. Annual average ^{137}Cs a) time integrated air concentration, b) dry deposition, and c) wet deposition fields (on a logarithmic scale) as a function of radial distance from the Leningrad NPP.

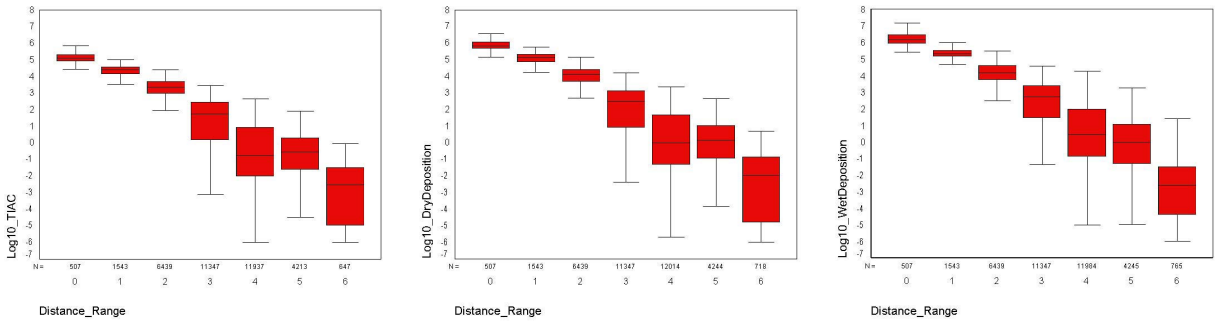

(a) (b) (c)

Figure 3.4.4. Box-plots of the annual average ^{137}Cs patterns distribution for the a) time integrated air concentration, b) dry deposition, and c) wet deposition fields for the Leningrad NPP as a function of the distance class (0 - <500km, 1 – 500-1000km, 2 – 1000-2000km, 3 - 2000-3000km, 4 – 3000-4000km, 5 – 4000-5000km, 6 – >5000km).

On a seasonal scale, as shown in Fig. 3.4.5, the highest magnitude TIAC isolines (1e+3 Bq·h/m^3) are concentrated around the sites and mostly they have a circle-oriented shape, although for the British site, during summer it is significantly extended in the eastern direction and during winter – in the north-western direction of the site (Fig. 3.4.5a). For the Ignalina site (Fig. 3.4.5b), during summer it is more extended in the western direction, and during winter - in eastern direction. The highest concentrations are more characteristic for the border regions of Lithuania, Latvia, and Belarus. For the NZS site, during all seasons it is more concentrated in the NW-SW sector of the site, and it is extended almost twice farther to the west compared with the east (Fig. 3.4.5c).

Similarly, the TIAC isolines of 1e+2 Bq·h/m^3 are more extended in the directions of main airflow from the sites and they have more an elliptical shape than a circle shape. For the BBP site (Fig. 3.4.5a) during atmospheric transport such concentrations were not even observed at the seashore of the European continent. These TIACs occurred mostly over the British Islands and

adjacent seas. For the Ignalina site (Fig. 3.4.5b), during summer the same isoline is more extended (almost twice) in the western direction than during winter – in opposite, eastern direction of the site. During spring, the extension is more pronounced along the NE-SW section. Among the Scandinavian countries, the TIAC can reach magnitudes of 1e+2 Bq·h/m^3 at the Baltic seashore counties of Sweden only during summer, and south of Finland - only during spring. For NZS site (Fig. 3.4.5c), during winter a significant extension in the NW direction from the site is occurred, and during summer the area of the TIAC field is almost twice larger compared with all other seasons. Throughout the year the populated Russian territories were practically unaffected by these levels of concentration. Moreover, the seasonal variability of the NZS TIAC field varied within a 5 degree latitudinal belt.

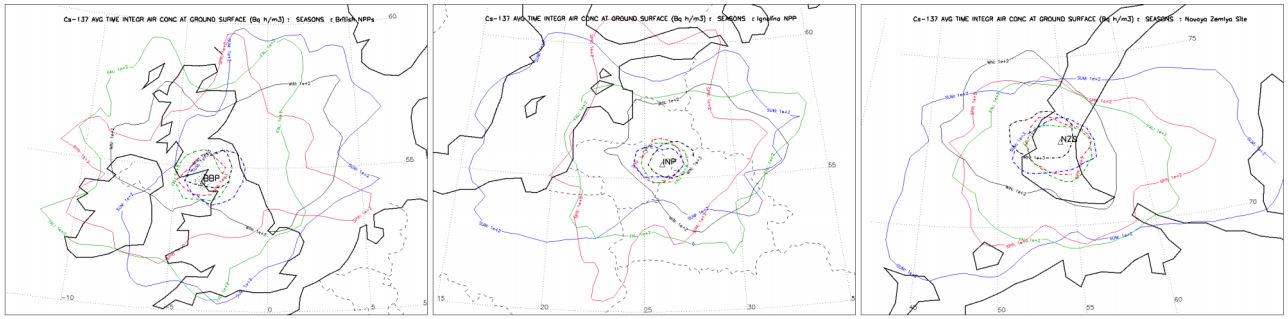

(a) (b) (c)

Figure 3.4.5. Seasonal average ^{137}Cs time integrated air concentration fields for the a) British NPPs, b) Ignalina NPP, and c) Novaya Zemlya test site.

The further analyses of the seasonal DD and WD fields for the same NRSs (shown in Figs. 3.4.6-3.4.8) showed a more complex structure of the calculated fields, especially of the WD fields. The dry deposition fields are significantly (especially during summer in the southern directions) extended in all directions from the sites compared with the TIAC fields. The WD showed fields with multiple cells. This reflected a cellular structure of the precipitation patterns. These fields are also farther extended compared with the DD fields.

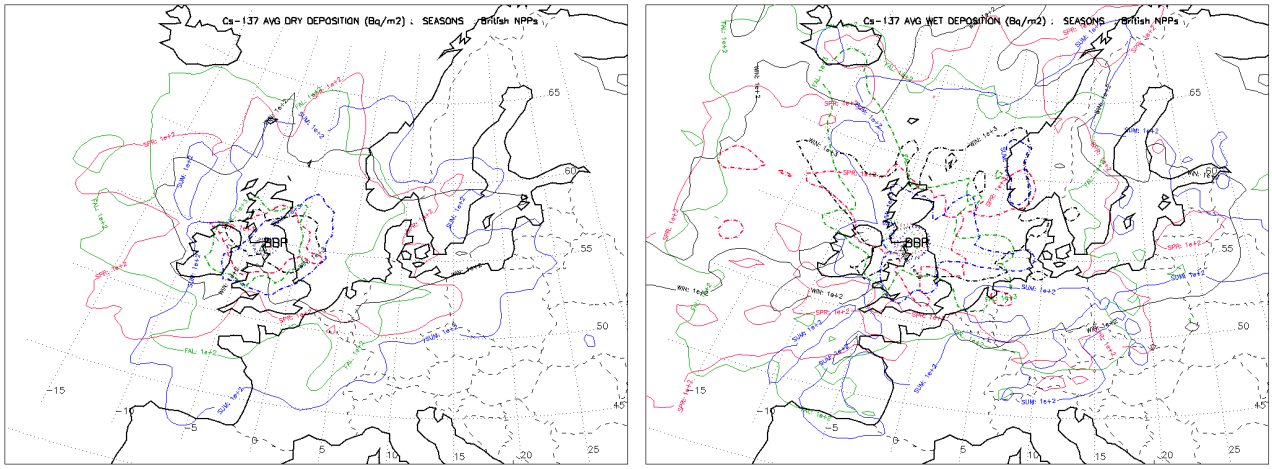

Figure 3.4.6. Seasonal average ^{137}Cs dry (left) and wet (right) deposition fields for the British NPPs (BBP).

In particular, the multiple cells structure of wet deposition is well seen during all seasons for the BBP site (Fig. 3.4.6) compared with the Ignalina and Novaya Zemlya sites. This multiplicity depends strongly on the maritime climate peculiarities of the BBP site. The wet depositions as higher as 1e+3 Bq/m^2 are observed during winter-summer in the western part of Norway, during

winter – in Denmark, during fall – in Iceland and western seashore territories of Germany and Benelux countries. The areas of wet depositions of 1e+2 Bq/m^2 are extended to the south passing at 45ºN and to the east passing at 30ºE.

The multiple cells structure of wet deposition is less pronounced for the Ignalina NPP (Fig. 3.4.7). This site is more attributed to the inland site, and hence, it is related to more continental type of the climate. During summer, although the dry deposition is higher in the E-S sector, the wet deposition is more characteristic for the territories northerly of the site. During winter, the areas enclosed by isolines of 1e+3 Bq/m^2 are almost 2.5 larger for WD compared with DD field, and these are more extended in the eastern directions from the site. Hence, throughout the year the dry deposition of 1e+3 Bq/m^2 is observed mostly over the Baltic States and northern Belarus. The wet deposition of the same order of magnitude is characteristic for a wider area, especially during winter, covering additionally territories of the Northwest Russia, Belarus, Ukraine, and Poland, as well as extending farther into the Baltic Sea aquatoria. Cells of the local maxima for WD are more often observed to the west of the site compared with the eastern directions (i.e. farther to the Eurasian continent).

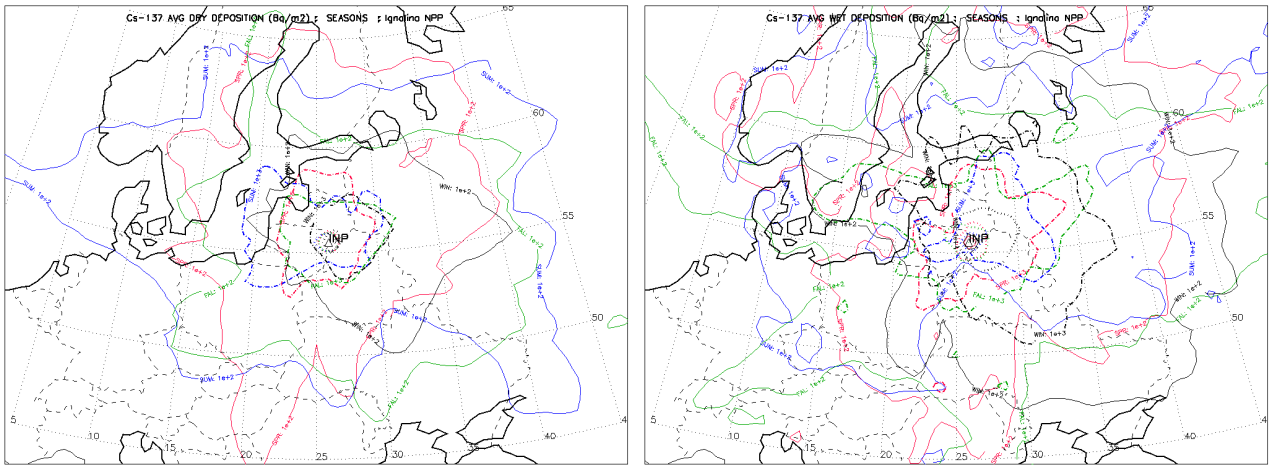

Figure 3.4.7. Seasonal average ^{137}Cs dry (left) and wet (right) deposition fields for the Ignalina NPP (INP).

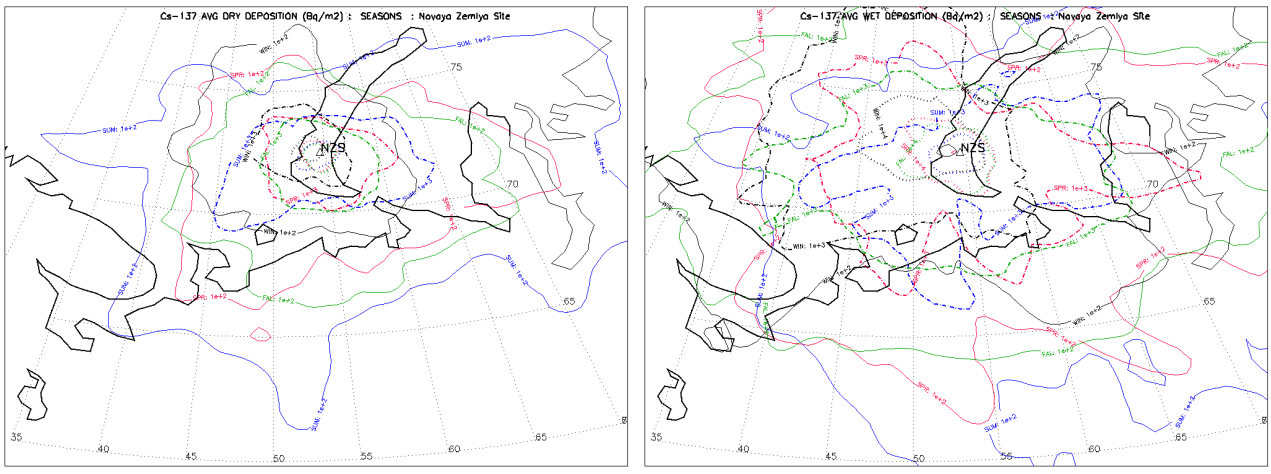

Figure 3.4.8. Seasonal average ^{137}Cs dry (left) and wet (right) deposition fields for the Novaya Zemlya test site (NZS).

For the Artic latitude site - Novaya Zemlya Archipelago (Fig. 3.4.8) - the wet deposition pattern showed less variability in precipitation patterns. Although the WD fields are more extended

in all directions from the site compared with the DD fields, they have no well underlined patterns of irregularity compared with other discussed sites. Throughout the year both depositions of 1e+3 Bq/m^2 and higher magnitudes are not observed over populated Russian territories. During summer, dry deposition of a lesser order of magnitude (1e+2 Bq/m^2) can be observed over the Murmansk and Archangelsk regions. The WD of the same magnitudes for the same regions is characteristic during all seasons, although during winter-fall the areas enclosed by these isolines are more extended farther to the Scandinavian Peninsula as well as during spring-summer they more extended to the south of the site (up to 60ºN) over populated Russian territories.

The analysis of seasonal variability of the ^{137}Cs WD patterns at selected cities (Tab. 3.4.1) showed that the deposition can be as much as 3.9 times higher during a particular season compared with the average annual deposition. This is a characteristic situation in Dublin, Ireland during fall. Among selected cities the lowest rate of maximum vs. average annual WD is 1.4 (Riga, Latvia). Moreover, the rate of more than 3.0 is observed for cities located farther than a 1500-km circle from the Leningrad plant. The minimum wet depositions are only characteristic during winter. This was observed at 17 among 26 cities selected, and all of these are located farther than 600-km of the site. The difference between the annual average and minimum varied up to 8 orders of magnitude at that time, although this difference was only up to one order of magnitude when a minimum was observed during other seasons.

Table 3.4.1. Seasonal variability of average ^{137}Cs wet deposition patterns (Bq/m^2) resulted from the hypothetical release at the Leningrad NPP at selected European cities.

City, Country	Dist to LNP, km	Spr	Sum	Fal	Win	Ann	Max (seas)	Max vs. Ann
Minsk, Belarus	673	2,79E+2	8,46E+1	2,30E+2	1,32E+2	1,81E+2	Spr	1,5
St.Petersburg, Russia	70	2,89E+4	1,68E+4	1,20E+4	8,03E+4	3,45E+4	Win	2,3
Moscow, Russia	686	8,32E+2	1,21E+2	5,80E+2	3,65E+2	4,75E+2	Spr	1,8
Kiev, Ukraine	1057	1,04E+1	1,26E+1	2,20E+2	4,58E+1	7,23E+1	Fal	2,9
Stockholm, Sweden	618	1,14E+2	1,19E+2	3,73E+2	3,32E+1	1,60E+2	Fal	2,3
Oslo, Norway	1014	2,54E+2	2,43E+2	1,31E+2	1,06E+1	1,60E+2	Spr	1,6
Helsinki, Finland	424	6,02E+1	5,71E+2	1,89E+3	4,78E+2	7,51E+2	Fal	2,5
Copenhagen, Denmark	1077	2,43E+1	1,59E+2	1,23E+2	2,12E-1	7,68E+1	Sum	2,1
Vienna, Austria	1535	1,34E+0	1,49E+0	5,43E+1	2,29E-4	1,43E+1	Fal	**3,8**
Paris, France	2095	1,15E+1	7,27E-1	5,52E-1	5,38E-5	3,20E+0	Spr	**3,6**
London, UK	2025	1,24E+1	4,52E+0	1,97E+1	3,34E-7	9,14E+0	Fal	2,2
Brussels, Belgium	1840	1,33E+1	1,12E+1	2,64E+0	1,62E-6	6,77E+0	Spr	2,0
Berlin, Germany	1261	1,87E+1	1,21E+2	6,56E+1	3,04E+0	5,21E+1	Sum	2,3
Budapest, Hungary	1522	1,58E+0	1,19E+0	1,42E+1	5,52E-2	4,26E+0	Fal	**3,3**
Bucharest, Romania	1731	4,21E+0	4,97E-1	1,07E+1	8,29E-1	4,07E+0	Fal	2,6
Warszawa, Poland	983	1,33E+1	5,23E+1	2,91E+1	6,32E-1	2,38E+1	Sum	2,2
Praha, Czech Republic	1426	9,94E-1	5,79E+1	5,11E+1	2,62E-2	2,75E+1	Sum	2,1
Bratislava, Slovakia	1515	2,38E+0	1,15E+1	4,09E+1	3,84E-3	1,37E+1	Fal	**3,0**
Luxembourg, Luxembourg	1845	1,91E+0	5,55E+0	8,85E+0	2,31E-5	4,08E+0	Fal	2,2
Amsterdam, Netherlands	1699	5,53E+0	1,30E+1	7,72E+0	1,66E-6	6,56E+0	Sum	2,0
Reykjavik, Iceland	2625	1,42E+0	6,10E-1	3,53E-1	9,87E-4	5,95E-1	Spr	2,4
Dublin, Ireland	2246	5,36E-2	2,03E-1	7,73E+0	2,05E-4	2,00E+0	Fal	**3,9**
Bern, Switzerland	2012	2,47E-1	1,78E+0	4,55E+1	6,78E-8	1,19E+1	Fal	**3,8**
Tallinn, Estonia	245	1,36E+2	6,37E+2	2,47E+3	1,30E+3	1,14E+3	Fal	2,2
Riga, Latvia	435	4,62E+2	1,68E+1	4,56E+2	3,09E+2	3,11E+2	Spr	1,4
Vilnius, Lithuania	622	1,14E+2	1,20E+2	2,36E+2	1,37E+2	1,52E+2	Fal	1,6

3.5. *INDICATORS OF NRS IMPACT FOR EMERGENCY RESPONSE AND PREPAREDNESS*

Information about probabilistic spatial and temporal distribution of concentration, dry and wet deposition patterns, especially during the fist day after an accident at NRS, could help the regional authorities and decision makers to plan more effectively the system of operational monitoring and emergency preparedness (i.e. to know: What areas are reachable during the first day after an accident occurred at NRS? When different regions, counties, administrative units, etc. should be ready for countermeasures after an accident/event at risk sites?). It should be noted that some estimates based on evaluation of only atmospheric transport from the sites were done by *Mahura & Baklanov, 2002*. They introduced a set of the NRS impact indicators to characterize peculiarities of the first day: fast transport (FT) probability fields, maximum reaching distance (MRD), maximum possible impact zone (MPIZ), and typical transport time (TTT) fields. Here, we will focus on estimates based on evaluation of both radionuclide transport and deposition patterns. Let us consider the British NRS as an example.

The annual average fields during the first day of atmospheric transport from the block of the British NPPs (BBP) are shown in Fig. 3.5.1a - for the time integrated air concentration of ^{137}Cs, in Fig. 3.5.1b – for the dry deposition of ^{137}Cs, and in Fig. 3.5.1c – for the wet deposition of ^{137}Cs. The seasonal variability of these three fields is shown in Fig. 3.5.2. The BBP site is geographically located on the British Islands. Hence, the atmospheric transport, dispersion, and deposition of radionuclides will strongly depend on the peculiarities of the maritime climate of these islands.

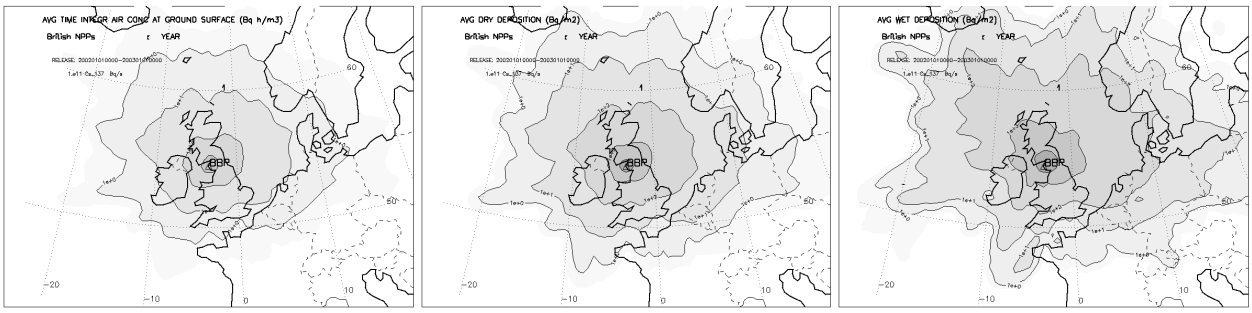

(a) (b) (c)

Figure 3.5.1. Annual average ^{137}Cs a) time integrated air concentration, b) dry deposition, and c) wet deposition fields during the first day of atmospheric transport from the British NPPs (BBP).

On an annual scale (Fig. 3.5.1), the higher values of concentration and depositions of ^{137}Cs are occurred more often to the north of the site compared with the southern directions. It is attributed to the prevailing atmospheric patterns associated with the Icelandic Low activities and proximity to the Gulf Stream current. For the WD field the annual areas, enclosed by the first three highest isolines of 1e+4, 1e+3, and 1e+2 Bq/m^2, are almost 2.5 times larger compared with the DD field. The higher values and larger areas for the wet deposition patterns, resulted from atmospheric transport from this site, depend on a frequent precipitation in this region as well as specifity of the maritime boundary layer which suppresses a deposition at the surface. During the first day, the British Islands and surrounding seas are mainly affected by the highest concentration and depositions ranging within 1e+3-1e+2 (Bq·h/m^3) and 1e+4-1e+3 (Bq/m^2), respectively. Among the populated European regions, only territories of countries situated along the seashore of the North Sea aquatoria, including Denmark, are at the higher risk compared with other countries. For most of the Western Europe countries, the TIAC of ^{137}Cs will be less than 1e+0 Bq·h/m^3, except Denmark, Northwest Germany, Benelux countries, and western territories of Norway. For the same territories,

the dry deposition is about of 1e+1 (Bq/m^2) and the wet deposition is twice higher (i.e. it is about of 1e+2 Bq/m^2).

Let us consider TIAC, DD, WD, and total deposition (TD) at selected geographical locations (capitals of the European countries situated northerly than 45ºN).

Table 3.5.1. Annual average ^{137}Cs time integrated air concentration, dry, wet, and total depositions during the first day of atmospheric transport at selected European cities resulted from the hypothetical release at the British NPPs.

#	City, Country	Dist to LNP, km	TIAC, Bq·h/m^3	DD, Bq/m^2	WD, Bq/m^2	TD, Bq/m^2	DD/ TD, %	WD/ TD, %
1	*Copenhagen, Denmark*	**1029**	1,18E+0	6,36E+0	6,25E+1	6,89E+1	9	**91**
2	*Helsinki, Finland*	1622	3,97E-5	2,15E-4	1,25E-3	1,46E-3	15	**85**
3	*Oslo, Norway*	**1045**	5,16E-1	2,79E+0	1,14E+1	1,42E+1	20	**80**
4	*Stockholm, Sweden*	**1406**	4,50E-2	2,43E-1	1,41E+0	1,65E+0	15	**85**
5	*Reykjavik, Iceland*	**1488**	1,24E-4	6,71E-4	1,22E-2	1,29E-2	5	**95**
6	*Torshavn, Faeroes*	**859**	1,73E+0	9,33E+0	5,25E+1	6,19E+1	15	**85**
7	*Nuuk, Greenland*	2847	0,00E+0	0,00E+0	0,00E+0	0,00E+0	0	0
8	Minsk, Belarus	2005	1,04E-2	5,59E-2	8,29E-1	8,85E-1	6	**94**
9	St.Petersburg, Russia	2095	6,09E-17	3,29E-16	9,18E-15	9,51E-15	3	**97**
10	Moscow, Russia	2577	0,00E+0	0,00E+0	0,00E+0	0,00E+0	0	0
11	Kiev, Ukraine	2324	5,59E-10	3,02E-9	1,42E-8	1,72E-8	18	**82**
12	Vienna, Austria	1540	4,75E-5	2,57E-4	2,67E-5	2,83E-4	91	9
13	Paris, France	**744**	4,07E-1	2,20E+0	5,55E+0	7,75E+0	28	**72**
14	London, UK	**402**	1,52E+1	8,22E+1	1,25E+2	2,07E+2	40	**60**
15	Brussels, Belgium	**667**	4,13E+0	2,23E+1	5,14E+1	7,37E+1	30	**70**
16	Berlin, Germany	**1136**	5,66E-1	3,06E+0	2,70E+1	3,01E+1	10	**90**
17	Budapest, Hungary	1751	1,71E-8	9,23E-8	1,29E-13	9,23E-8	100	0
18	Bucharest, Romania	2389	0,00E+0	0,00E+0	0,00E+0	0,00E+0	0	0
19	Warszawa, Poland	1636	3,81E-2	2,06E-1	4,27E+0	4,48E+0	5	**95**
20	Praha, Czech Republic	**1312**	5,06E-2	2,73E-1	2,42E+0	2,69E+0	10	**90**
21	Bratislava, Slovakia	1589	2,97E-4	1,60E-3	1,38E-4	1,74E-3	92	8
22	Luxembourg, Luxembourg	**852**	4,65E-1	2,51E+0	1,59E+1	1,84E+1	14	**86**
23	Amsterdam, Netherlands	**606**	7,53E+0	4,06E+1	2,38E+2	2,78E+2	15	**85**
24	Dublin, Ireland	**222**	6,16E+1	3,33E+2	3,26E+2	6,58E+2	51	49
25	Bern, Switzerland	**1141**	1,22E-4	6,56E-4	1,43E-2	1,50E-2	4	**96**
26	Tallinn, Estonia	1781	4,42E-7	2,39E-6	1,88E-5	2,12E-5	11	**89**
27	Riga, Latvia	1737	1,27E-3	6,83E-3	2,64E-1	2,71E-1	3	**97**
28	Vilnius, Lithuania	1844	1,90E-2	1,03E-1	3,66E+0	3,76E+0	3	**97**
29	**BBP, UK**	***0***	4,48E+3	2,42E+4	2,53E+4	4,95E+4	49	**51**

As seen from Tab. 3.5.1 the highest values for the concentration and depositions (1e+3 and 1e+4 orders of magnitude, respectively) are in vicinity of the BBP site. During the first day the contribution of the wet deposition into the total deposition is several times higher for most of the selected cities, except Vienna and Bratislava. The WD contribution is almost equal to the DD contribution at Dublin and the BBP site. For three cities – Moscow, Nuuk, and Bucharest – for both contributions it is equal to 0 (i.e. cities were not reachable during the first day of atmospheric transport) because the limited duration (5-days) of trajectories considered. For cities situated within a 1000-km circle around the BBP site, the concentration decreased by several orders of magnitude: from 1e+3 to 1e-1 Bq·h/m^3.

On a seasonal scale (Fig. 3.5.2), during summer the areas of the TIAC, DD, and WD fields are smaller compared with other seasons, and they are more concentrated around the BBP site. Moreover, these fields are also less extended in the eastern sector from the site, although in other seasons there is a significant propagation of the isolines in the eastern directions. During fall, the Scandinavian Peninsula countries are minimally affected by atmospheric transport and deposition from the site, the contours of the fields are more extended in the NW-SE direction (passing over the Faeroe Islands and Scandinavian countries) compared with others. During winter, the WD pattern is significantly propagated in the inland European countries.

Finally, analysis of such TIAC, DD, and WD fields could be used in the emergency response systems for accidental releases of radioactivity. These fields allow an estimation of transport times, boundaries of possible maximal contamination, integrated concentrations, dry and wet deposition patterns, geographically farthest territories reachable by a contaminated cloud during selected time (for example, every 3 hour) atmospheric transport from the risk sites to/over a particular geographical territory, region, country, city, etc. This information is one of the important input parameters for the decision-making process.

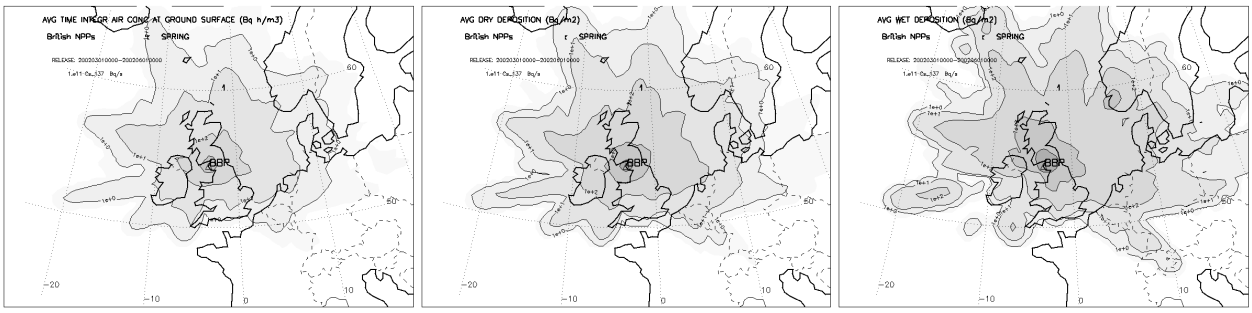

(Spr) (Spr) (Spr)

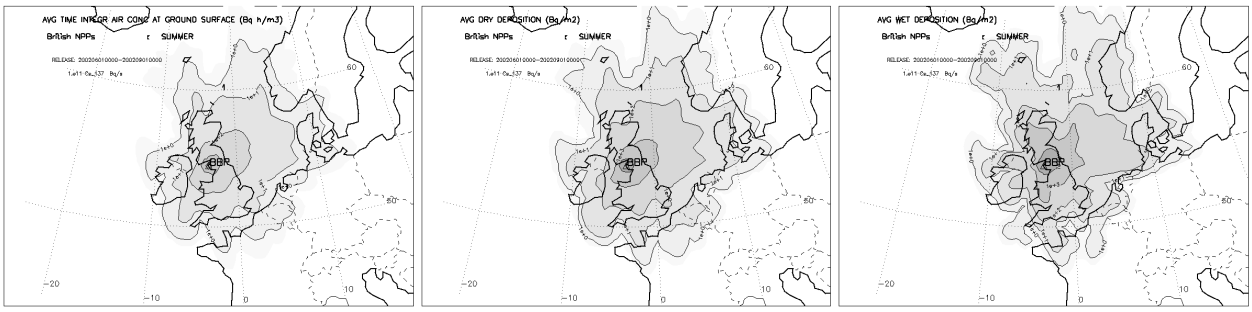

(Sum) (Sum) (Sum)

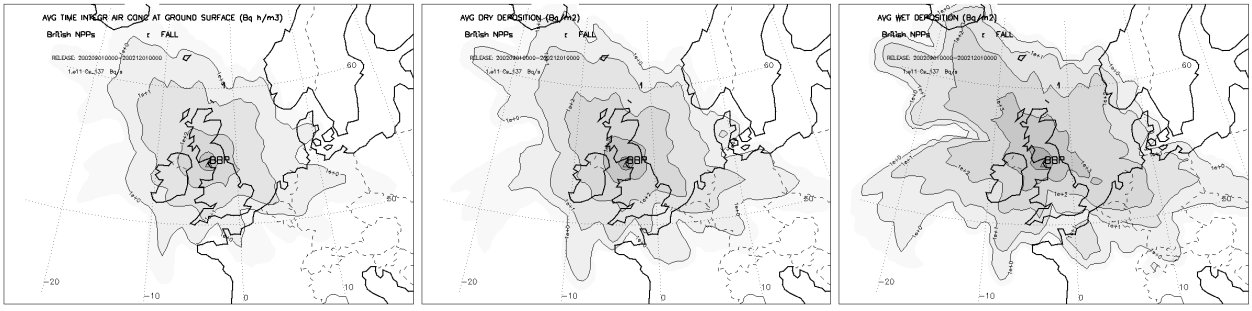

(Fal) (Fal) (Fal)

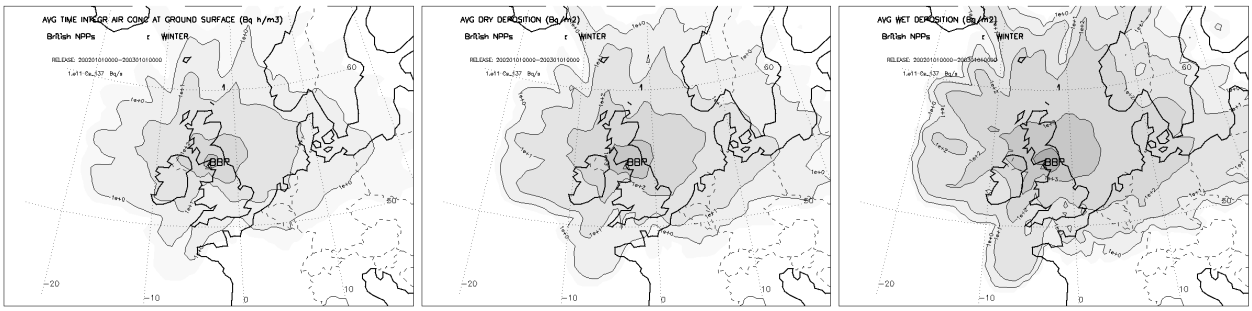

(Win) (Win) (Win)

Figure 3.5.2. Seasonal average ^{137}Cs time integrated air concentration (left), dry deposition (middle), and wet deposition (right) fields during the first day of atmospheric transport from the British NPPs.

It should be reminded also that the BBP site consisted of several nuclear risk sources including the Sellafield nuclear processing plant. Hence, the results obtained for the BBP site will be similar if modelling will be performed for the exact geographical location of the mentioned processing plant. It is assumed to be valid due to short distance between the coordinates of the BBP site and Sellafield plant as well as due to similarities of the characteristic mesoscale patterns over the geographical region of both sites' locations.

3.6. *SPECIFIC CASE STUDIES FOR ^{137}CS, ^{131}I, ^{90}SR, AND ^{85}KR RELEASES*

In comparison with the long-term dispersion modelling, the specific case studies have some peculiarities and criteria for selection discussed by *Baklanov et al., 2002b.* The specific case study approach is computationally less expensive compared with the dispersion modelling for a multiyear period, although it allows considering further risk and vulnerability analysis only on particular dates. Alternatively, this approach provides possibility to see potential consequences of an accident for worst-case meteorological situations. Some case studies with evaluation of possible consequences were considered for the Kola nuclear power plant (*Baklanov et al., 2002a*) and nuclear submarine bases of the Russian Northern and Pacific Fleets (*Bergman et al., 1998; Baklanov et al., 2002b; Mahura et al., 2002; Baklanov et al., 2003*).

The selection of specific cases with typical or worst-case scenarios can be based on results from trajectory modelling and probability fields analysis. In general, at least, four *criteria* could be used for specific case selection. *First*, the direction of atmospheric transport of radioactive cloud after an accidental release at NRS should be toward the region of interest. In our study, these regions are countries and populated territories of the Euro-Arctic region. *Second*, the possibility of precipitation during atmospheric transport of the radioactive cloud over the region of interest should be taken into account. In our study it could be inferred from the dispersion modelling of wet deposition patterns. *Third*, the relatively short travel time of the radionuclide cloud from the NRS location toward the region of interest will be important. *Fourth*, the relatively large coverage of the regions of interest by the radioactive cloud during atmospheric transport should be considered.

In this section of report, we will consider two specific cases in more details. These cases are: A) 24th August 2000, and B) 10th April 2002. For these cases, we evaluated atmospheric transport, dispersion, and deposition of the following radionuclides - ^{137}Cs, ^{131}I, ^{90}Sr, ^{95}Kr - for the discrete continuous unit hypothetical release (DUHR) with a fixed rate of $1{\cdot}10^{11}$ Bq/s. Hence, the total amount of radioactivity released during a one-day release is equal to $1{\cdot}10^{11}$(Bq/s)·24(hour)·60(min)·60(sec) = $8.64{\cdot}10^{15}$ (Bq). For simplification let us suggest this

amount to be the same for all radionuclides. We do not consider any specific accident scenario but our simulation results can be easily recalculated for any scenario of accident. Moreover, we did not consider different release heights because such sensitivity studies were done by *Bergman et al., 1998*; *Baklanov et al., 2001*.

Specific Case A: Leningrad NPP, 24 August 2000

For this specific case of 24 August 2000, we analyzed atmospheric transport of three radionuclides (^{137}Cs, ^{131}I, and ^{90}Sr – as major dose-contributing radionuclides) for DUHR occurred during 24 hours (24-25 Aug 2000, 00 UTC) at the Leningrad NPP, Russia. As input meteorological data the ECMWF model output was used. Following the subsequent temporal daily snapshots of radionuclide concentration it is possible to identify propagation of the radionuclide cloud.

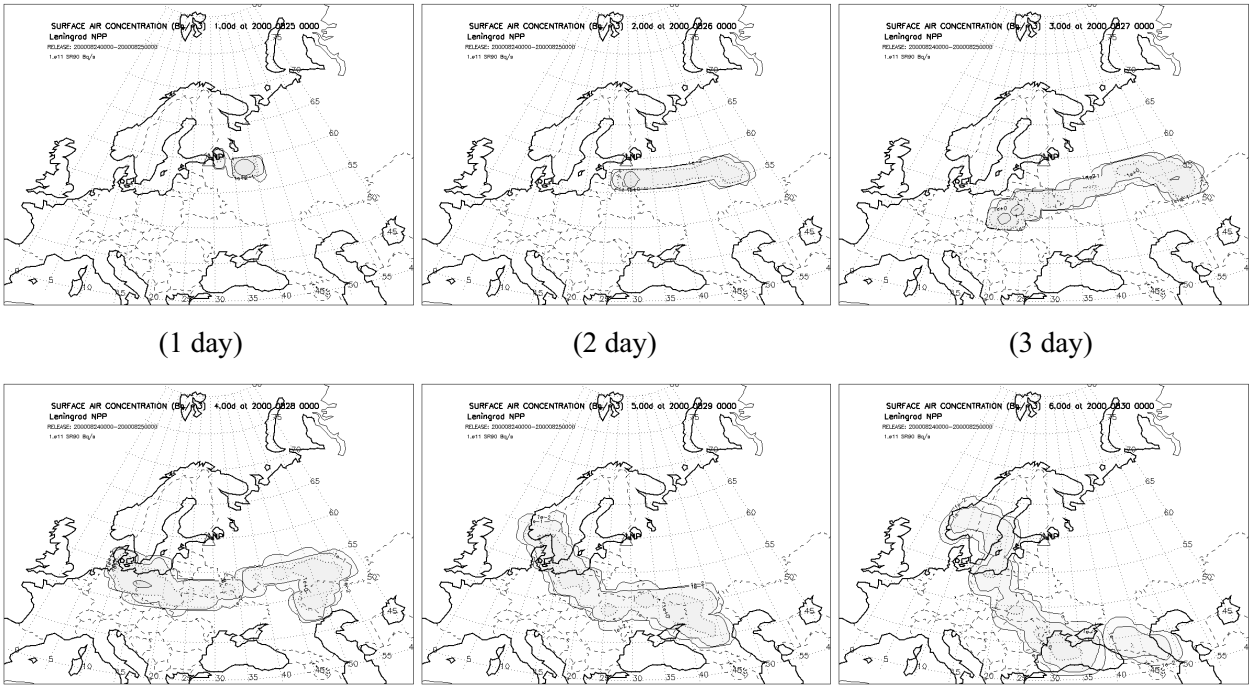

Figure 3.6.1. ^{90}Sr air concentration fields for DUHR occurred during 24-25 Aug 2000, 00 UTC from the Leningrad NPP.

During the first two days, atmospheric transport generally occurred in the eastern direction from the site as shown in Figs. 3.6.1 and 3.6.2 for ^{90}Sr and ^{131}I, respectively. During the 3rd day, the contaminated cloud continued motion by westerlies, although a transport in the western direction is also became pronounced. During the 4th day, since release occurred at the LNP site, the directions of the separated cloud transport did not change significantly, except that the southern component became evident. During the 5th and 6th days, a part of the radionuclide cloud, initially moved in the eastern direction, propagated to the south passing over territories of the Black Sea and Ukraine. Other part of the cloud, previously moved in the western direction, travelled to the north passing over territories of the Scandinavian countries.

Comparison of ^{90}Sr and ^{131}I (long-lived vs. short-lived radionuclide) showed a significant decrease of concentration during atmospheric transport. This especially is seen at the last two days (5 and 6). Only small areas over the Scandinavian Peninsula and Black Sea were still affected by

the presence of ^{131}I on the 6th day, although for ^{90}Sr, the affected area remained relatively large extending from the southern territories of the Scandinavian Peninsula to the Black Sea.

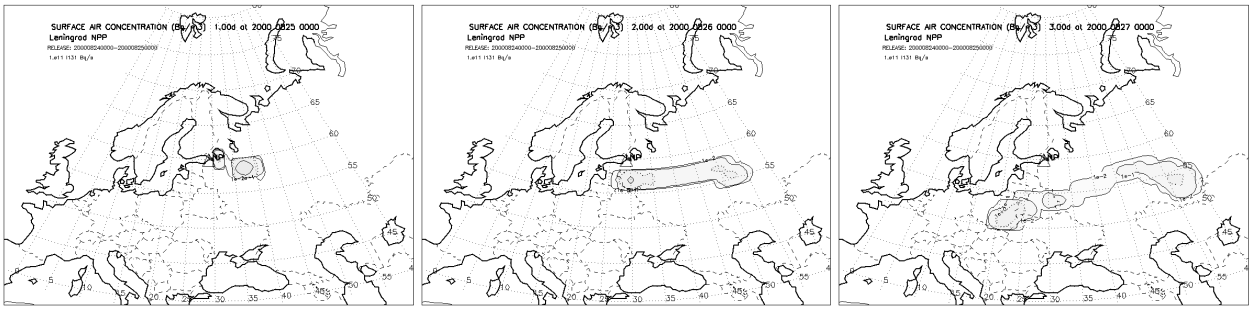

(1 day) (2 day) (3 day)

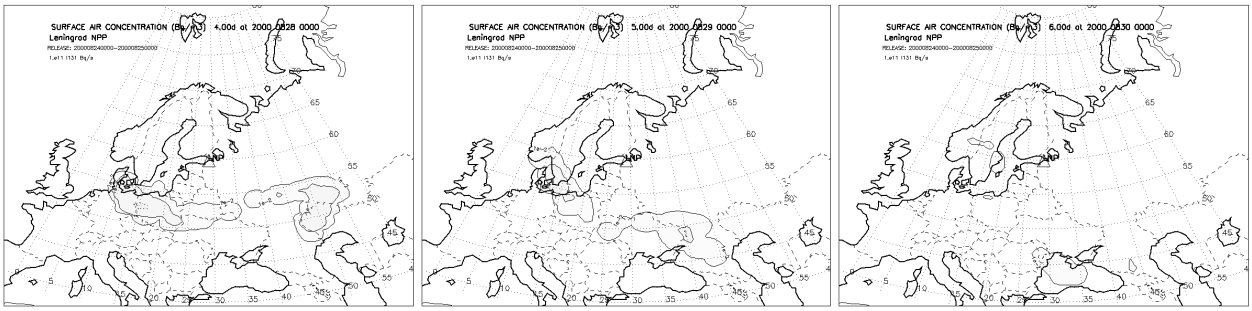

(4 day) (5 day) (6 day)

Figure 3.6.2. ^{131}I air concentration fields for DUHR occurred during 24-25 Aug 2000, 00 UTC from the Leningrad NPP.

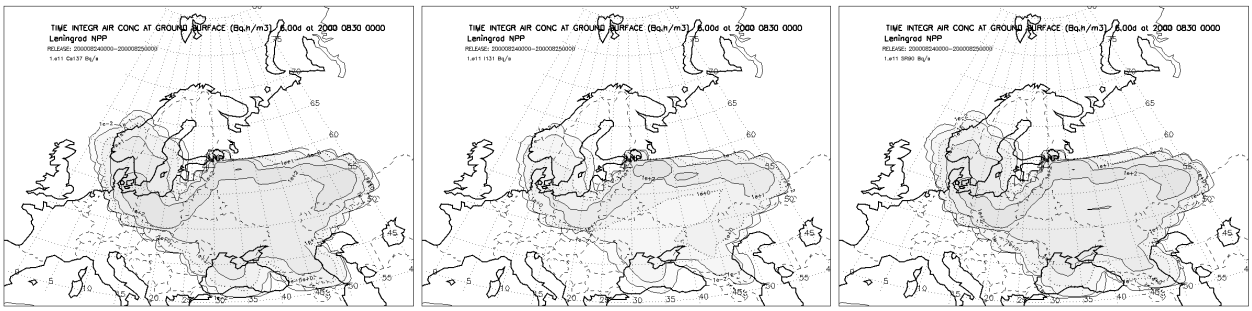

(a) (b) (c)

Figure 3.6.3. Time integrated air concentration fields of a) ^{137}Cs, b) ^{131}I, and c) ^{90}Sr on 6th day of atmospheric transport from the Leningrad NPP for DUHR occurred during 24-25 Aug 2000, 00 UTC.

The TIAC fields for all three radionuclides are shown in Fig. 3.6.3. The shape and structure of TIAC are similar for nuclides: ^{137}Cs and ^{90}Sr. The correlation coefficient between these two fields is 0.98. It is not a surprise because it is strongly dependent on the half-life of the nuclides ($9.50428 \cdot 10^8$ sec vs. $9.17640 \cdot 10^8$ sec for ^{137}Cs vs. ^{90}Sr, respectively) used in modelling of radioactive decay processes. Similar conclusion can be made about the DD fields shown in Fig. 3.6.4. Since the Leningrad NPP site is an inland site, the more continental type of the climate than the maritime is a peculiarity of this site compared, for example, with the Sellafield processing plant (discussed in §3.5). The strong dependence on the precipitation irregularity presence during

atmospheric transport of the contaminated cloud is reflected in the wet deposition patterns. Hence, the structure of the WD field is more cellular compared with TIAC and DD. The total area enclosed by the WD isolines is much smaller too (Fig. 3.6.5).

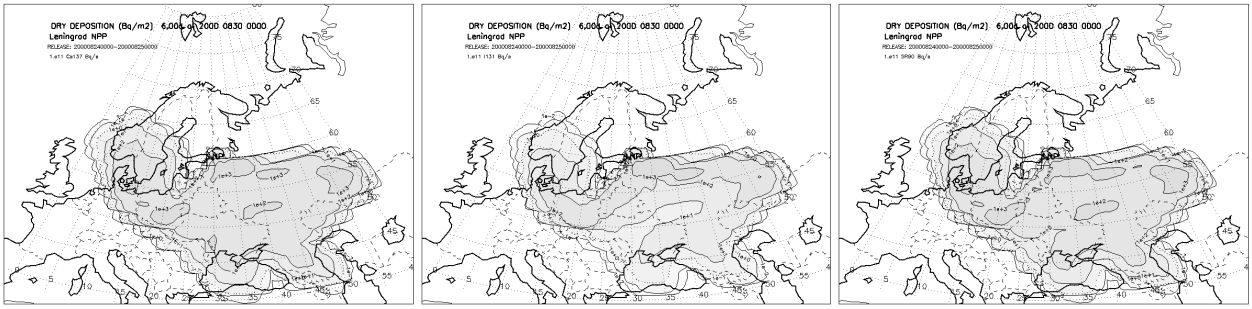

(a) (b) (c)

Figure 3.6.4. Dry deposition fields of a) ^{137}Cs, b) ^{131}I, and c) ^{90}Sr on 6th day of atmospheric transport from the Leningrad NPP for DUHR occurred during 24-25 Aug 2000, 00 UTC.

Analyses of fields (shown in Figs 3.6.1-3.6.5) allow identifying several features for this specific case. First, it should be noted that for ^{137}Cs and ^{90}Sr the shape and magnitude of isolines are similar for all fields, and it is due to almost the same half-life times and reference dry deposition velocities for these radionuclides compared with ^{131}I. Second, for ^{131}I, the surface air concentration decreases faster with distance from the site (similar with other calculated fields, although the rate of decrease is slower). Additionally, an area under a particular order of magnitude isoline could be calculated similarly to estimation of areas enclosed by isolines of the maximum reaching distance and maximum possible impact zone indicators (based on results of trajectory modelling, see *Mahura & Baklanov, 2002*).

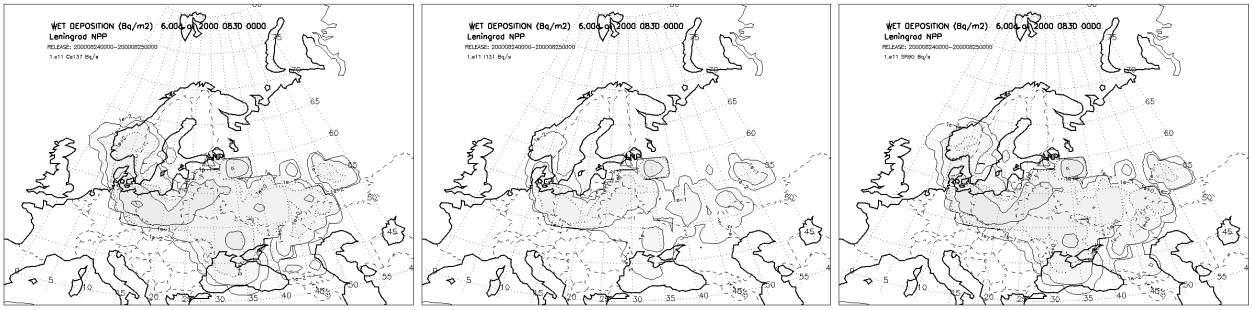

(a) (b) (c)

Figure 3.6.5. Wet deposition fields of a) ^{137}Cs, b) ^{131}I, and c) ^{90}Sr on 6th day of atmospheric transport from the Leningrad NPP for DUHR occurred during 24-25 Aug 2000, 00 UTC.

If several geographical locations of interest are selected (i.e. its latitude and longitude are known) than exact values of the time integrated air concentration, dry deposition, and wet deposition can be calculated by interpolation from the original fields. Let us evaluate TIAC, DD, and WD (shown in Tab. 3.6.1 and 3.6.2) at locations of the selected European cities after 5 days of atmospheric transport from the Leningrad NPP.

The highest ^{137}Cs TIAC (1.61e+2 Bq·h/m^3) was at Copenhagen, Denmark and the lowest – 4.95e-4 Bq·h/m^3 - was at Riga, Latvia. Similarly, the highest ^{90}Sr TIAC – 1.16e+2 Bq·h/m^3 - at Copenhagen, Denmark, and the lowest - 2.98e-4 Bq·h/m^3 - at Riga, Latvia. But, although the lowest

^{131}I TIAC (3.33e-6 Bq·h/m^3) was at Riga, Latvia; the highest – 1.74e+1 Bq·h/m^3 - at Minsk, Belarus. The similar situation is for the DD patterns vs. radionuclides, i.e. the highest and lowest magnitudes of DD for a particular radionuclide were observed at the same cities as for the concentrations. The lower TIACs and DDs for three cities – Budapest, Tallinn, and Riga – is a result of latter arrival of the contaminated cloud to these locations compared with other cities.

Table 3.6.1. Estimated time integrated air concentration of radionuclides at selected cites for DUHR occurred (24-25 Aug, 2000, 00 UTC) at the Leningrad NPP.

City, Country	Lat, °	Long, °	Distance to LNP, km	Time Integrated Air Concentration (TIAC), Bq·h/m^3		
				^{137}Cs	^{131}I	^{90}Sr
St.Petersburg, Russia	59.89	30.26	**70**	9,49E+0	8,48E+0	9,39E+0
Tallinn, Estonia	59.43	24.73	**245**	1,86E-3	9,87E-6	1,10E-3
Helsinki, Finland	60.60	21.43	**424**	5,50E-1	3,03E-3	3,24E-1
Riga, Latvia	56.95	24.10	**435**	4,95E-4	3,33E-6	2,98E-4
Stockholm, Sweden	59.33	18.05	**618**	1,52E+1	1,81E-1	9,67E+0
Vilnius, Lithuania	54.67	25.32	**622**	6,72E+1	1,30E+1	5,69E+1
Minsk, Belarus	53.90	27.57	**673**	1,21E+2	1,74E+1	9,88E+1
Moscow, Russia	55.75	37.58	**686**	3,48E+1	5,00E+0	2,82E+1
Warszawa, Poland	52.25	21.00	**983**	1,41E+2	8,10E+0	1,03E+2
Oslo, Norway	59.92	10.75	**1014**	2,60E+1	5,15E-1	1,76E+1
Kiev, Ukraine	50.43	30.52	**1057**	3,13E+1	5,19E-1	2,06E+1
Copenhagen, Denmark	55.67	12.58	**1077**	1,61E+2	6,23E+0	1,16E+2
Berlin, Germany	52.52	13.40	**1261**	1,36E+2	8,57E+0	1,03E+2
Praha, Czech Republic	50.08	14.47	**1426**	3,91E+0	3,16E-1	3,04E+0
Bratislava, Slovakia	48.15	17.12	1515	4,82E-2	4,54E-3	3,80E-2
Budapest, Hungary	47.50	19.08	1522	2,61E-3	9,55E-6	1,47E-3
Vienna, Austria	48.20	16.37	1535	6,65E-3	5,85E-4	5,22E-3
Bucharest, Romania	44.43	26.10	1731	1,30E-1	1,24E-3	8,18E-2

Table 3.6.2. Estimated dry and wet depositions, and percentage contribution of wet deposition of radionuclides at selected cites for DUHR occurred (24-25 Aug, 2000, 00 UTC) at the Leningrad NPP.

City, Country	Dry Deposition (Bq/m^2)			Wet Deposition (Bq/m^2)			Wet Deposition/ Total Deposition, %		
	^{137}Cs	^{131}I	^{90}Sr	^{137}Cs	^{131}I	^{90}Sr	^{137}Cs	^{131}I	^{90}Sr
St.Petersburg, Russia	5,13E+1	1,18E+2	6,76E+1	9,85E-2	5,72E-2	9,75E-2	0,2	<0,1	0,1
Tallinn, Estonia	1,01E-2	2,11E-4	7,90E-3	0,00E+0	0,00E+0	0,00E+0	<0,1	<0,1	0,0
Helsinki, Finland	2,97E+0	6,50E-2	2,33E+0	3,31E-3	1,82E-5	1,95E-3	0,1	<0,1	0,1
Riga, Latvia	2,67E-3	6,93E-5	2,15E-3	7,63E-7	3,76E-9	4,45E-7	<0,1	<0,1	<0,1
Stockholm, Sweden	8,20E+1	3,84E+0	6,96E+1	9,99E-5	2,92E-6	7,08E-5	<0,1	<0,1	<0,1
Vilnius, Lithuania	3,63E+2	2,07E+2	4,09E+2	3,34E+1	5,06E+0	2,84E+1	8,4	2,4	6,5
Minsk, Belarus	6,51E+2	2,83E+2	7,11E+2	3,92E+1	4,59E+0	3,25E+1	5,7	1,6	4,4
Moscow, Russia	1,88E+2	7,85E+1	2,03E+2	1,38E-2	5,09E-4	1,01E-2	<0,1	<0,1	<0,1
Warszawa, Poland	7,64E+2	1,43E+2	7,42E+2	8,62E+0	4,44E-1	6,47E+0	1,1	0,3	0,9
Oslo, Norway	1,40E+2	1,05E+1	1,26E+2	1,20E+0	2,13E-2	8,05E-1	0,8	0,2	0,6
Kiev, Ukraine	1,69E+2	1,01E+1	1,49E+2	4,25E+0	6,03E-2	2,79E+0	2,5	0,6	1,8

Copenhagen, Denmark	8,68E+2	1,20E+2	8,36E+2	9,75E+0	4,14E-1	7,21E+0	1,1	0,3	0,9
Berlin, Germany	7,32E+2	1,57E+2	7,41E+2	7,87E+1	4,57E+0	6,03E+1	9,7	2,8	7,5
Praha, Czech Republic	2,11E+1	5,63E+0	2,19E+1	1,50E+0	1,03E-1	1,17E+0	6,6	1,8	5,1
Bratislava, Slovakia	2,60E-1	7,87E-2	2,74E-1	6,71E-3	4,91E-4	5,28E-3	2,5	0,6	1,9
Budapest, Hungary	1,41E-2	2,05E-4	1,06E-2	1,56E-4	5,53E-7	8,78E-5	1,1	0,3	0,8
Vienna, Austria	3,59E-2	1,03E-2	3,75E-2	2,28E-3	1,64E-4	1,79E-3	6,0	1,6	4,6
Bucharest, Romania	7,04E-1	2,66E-2	5,89E-1	1,26E-3	1,19E-5	7,90E-4	0,2	<0,1	0,1

The highest ^{137}Cs WD (7.87e+1 Bq/m^2) was at Berlin, Germany and the lowest (7.63e-7 Bq/m^2) was at Riga, Latvia (considering that at Tallinn, Estonia the wet deposition did not even occur). Similarly, the highest ^{90}Sr WD (6.03e+1 Bq/m^2) - at Berlin, Germany and the lowest – 4.45e-7 Bq/m^2 - at Riga, Latvia. But, although the lowest ^{131}I WD (3.76e-9 Bq/m^2) was at Riga, Latvia, the highest – 5.06e+0 Bq/m^2 - at Vilnius, Lithuania. For this specific case, the contribution of wet deposition during atmospheric transport was, in general, negligible ranging from less than 0.1 (shown in Tab. 3.6.2 as <0.1 or negligible) to 9.7% of the total deposition. Because of the natural (following the radioactive decay) faster decrease of ^{131}I TIAC, especially during the first days of transport, the TIAC, DD, WD, and contribution of wet deposition were also several times lesser compared with other radionuclides. Hence, for this particular specific case the precipitation factor was not a significant contributor, and major role was played by the atmospheric transport, diffusion, and dry deposition.

Specific Case B: Chernobyl NPP, 10 April 2002

For this specific case of 10 Apr 2002, we analyzed atmospheric transport of three radionuclides (^{137}Cs, ^{131}I, and ^{85}Kr) for the discrete unit hypothetical releases (DUHR) of two variants occurred within 10-11 Apr 2002 at the Chernobyl NPP, Ukraine. As input meteorological data the DMI-HIRLAM model output was used. For comparative purposes two versions of the DMI-HIRLAM model were run: E-version (resolution of 0.15º) and G-version (resolution of 0.45º) - as shown in Figs. 3.6.6-3.6.7. Also, the hypothetical releases of two different durations were also studied: 24 hours (variant 1) and 3 hours (variant 2) occurred during 10-11 Apr 2002 – as shown in Figs. 3.6.6-3.6.7. The total amount of radioactivity released during 3 hours is equal to 3.78·10^{14} Bq, and for 24 hour release – 8.64·10^{15} Bq.

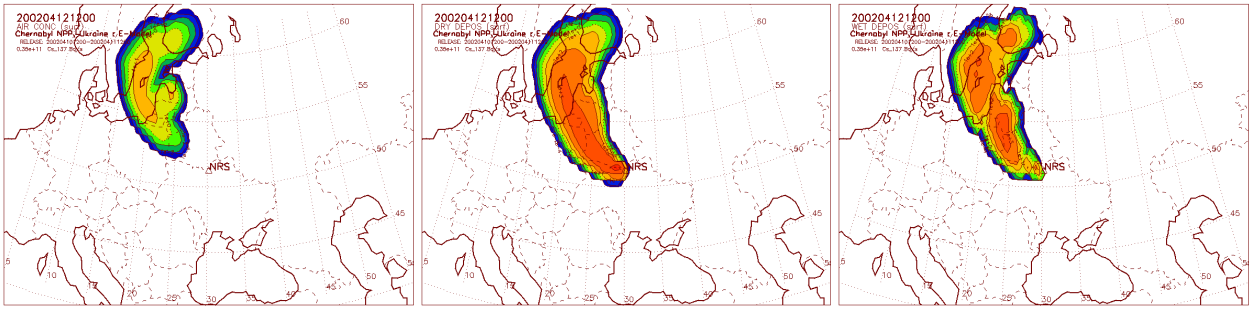

(E-version of the DMI-HIRLAM model)

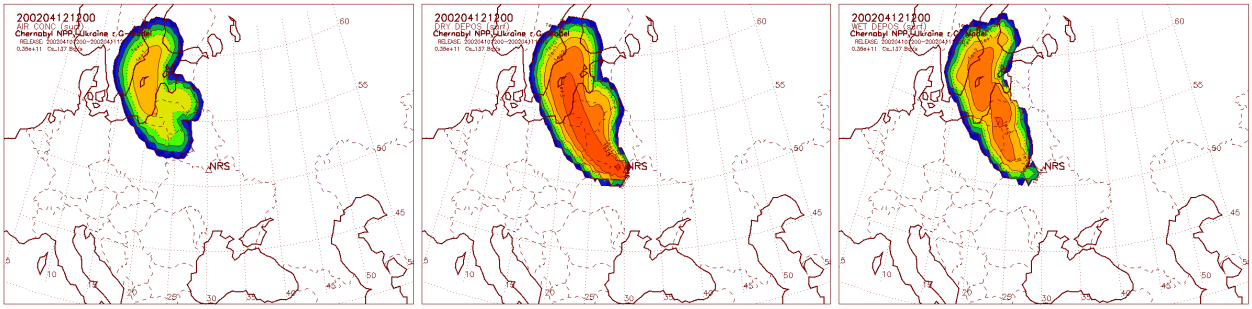

(G-version of the DMI-HIRLAM model)

Figure 3.6.6. ^{137}Cs air concentration (left), dry deposition (middle), and wet deposition (right) fields at 12 Apr 2002, 12 UTC for DUHR occurred during 24 hours (10-11 Apr 2002, 12 UTC) at the Chernobyl NPP.

The snapshots of calculated fields for the radionuclide ^{137}Cs air concentration, dry deposition, and wet deposition were taken after 2 days of atmospheric transport (i.e. at 12 Apr 2002, 12 UTC) since releases of both durations started at the Chernobyl site (i.e. at 10 Apr 2002, 12 UTC). During these two days, this specific case clearly showed the atmospheric transport in the north-western direction and deposition over territories of Belarus, eastern Poland, Baltic States, and southern parts of Sweden and Finland. After the first two days transport continued over the Scandinavian Peninsula and regions of the North-West Russia. Considering the similar magnitude isolines, it is well seen that the total area covered by the contaminated cloud is larger when a longer duration release is evaluated. In particular, the area of ^{137}Cs air concentration field (left plate in Fig. 3.6.7) is more than two times smaller compared with one day release (left plat in Fig. 3.6.6).

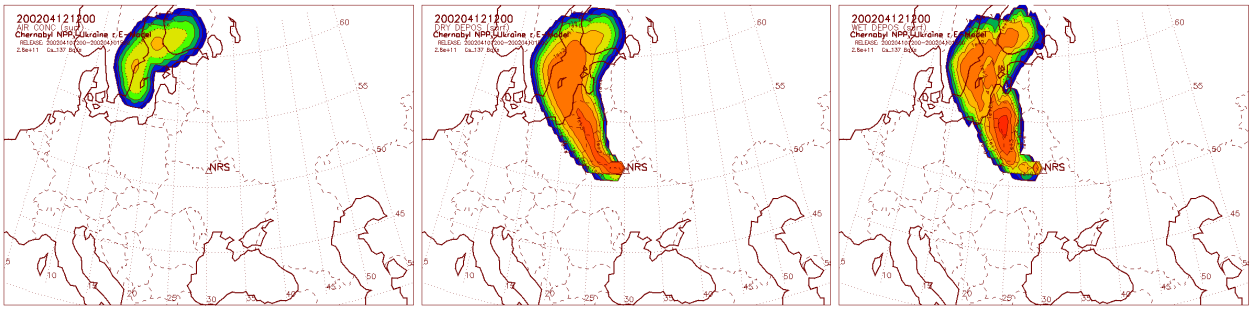

(E-version of the DMI-HIRLAM model)

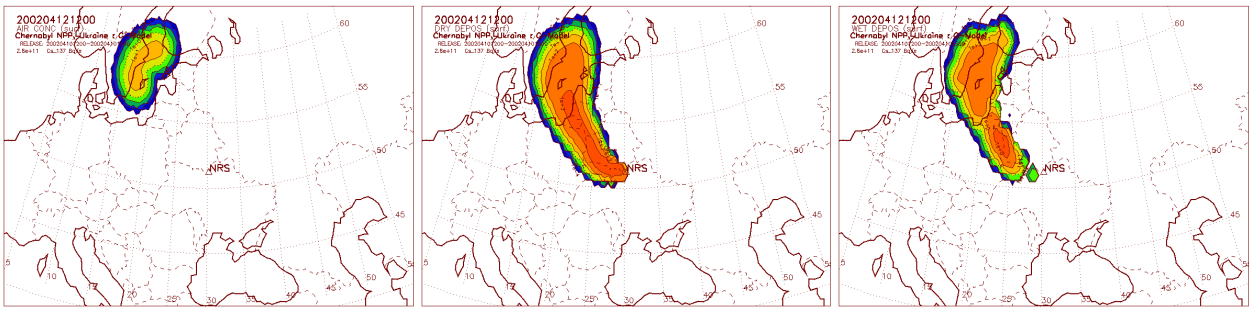

(G-version of the DMI-HIRLAM model)

Figure 3.6.7. ^{137}Cs air concentration (left), dry deposition (middle), and wet deposition (right) fields at 12 Apr 2002, 12 UTC for DUHR occurred during 3 hours (10 Apr 2002, 12-15 UTC) at the Chernobyl NPP.

Similarly, although less pronounced, the areas are larger for the dry and wet deposition fields shown in the middle and right plates of the same figures. It should be noted that the dry and wet deposition fields resemble each other by the shape, although the wet deposition field has more cellular structure, due to irregularity of rainfall patterns during transport over the studied region. The differences in the shapes of all patterns (considering results of the E and G versions), especially of the wet deposition pattern, strongly depend on the model resolution. In particular, in E-version the precipitation processes during atmospheric transport will be resolved more accurate, although in G-version these fields are more smoothed loosing some aspects of the rainfall irregularity.

The air concentration fields for three selected radionuclides at different time intervals for a one day release are shown in Fig. 3.6.8. The snapshots are given at 12, 13, and 14 Apr of 2002, 12 UTC. As seen from the figure, initially the atmospheric transport from the nuclear plant occurred in the north-western direction passing over territories of Belarus, Poland, and Baltic States. At 12 Apr 2002, the contaminated cloud reached an aquatoria of the Baltic Sea. During the next day - 13 Apr 2002 – the transport shifted in the northern, and then in the north-eastern directions passing over the aquatoria of the Baltic Sea and surrounding sea countries of the Scandinavian Peninsula and Baltic region. During the fourth day – 14 Apr 2002 – the cloud continued extension in the western and north-eastern directions passing over the Scandinavian Peninsula territories.

As seen from the figure, during the first days of transport the air concentration of ^{131}I decreased significantly compared with other nuclides. Concentration of this nuclide varied between 1e-3-1e-2 Bq·h/m^3 after 4 days of transport since release started at the site. The highest concentration is observed over the central aquatoria of the Baltic Sea and territories of Sweden and Finland adjacent to this aquatoria. Similar area with higher concentrations is for ^{137}Cs, although the concentration levels will be two orders of magnitude higher. Because ^{85}Kr, as a noble gas, does not account deposition processes during transport, the highest – 1e+1 Bq·h/m^3 - concentration of krypton remained if compared with other nuclides, as well as the area enclosed by the isolines remained the largest.

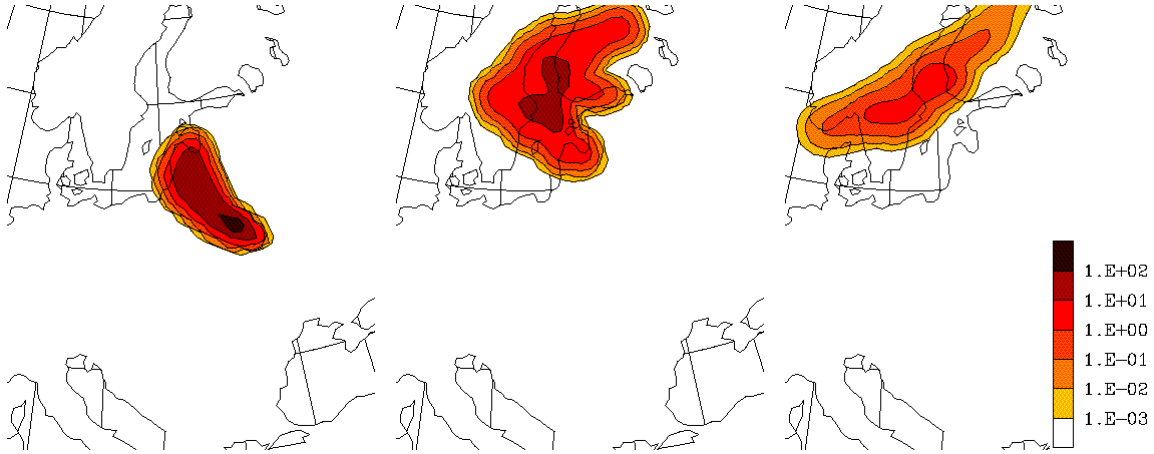

^{137}Cs

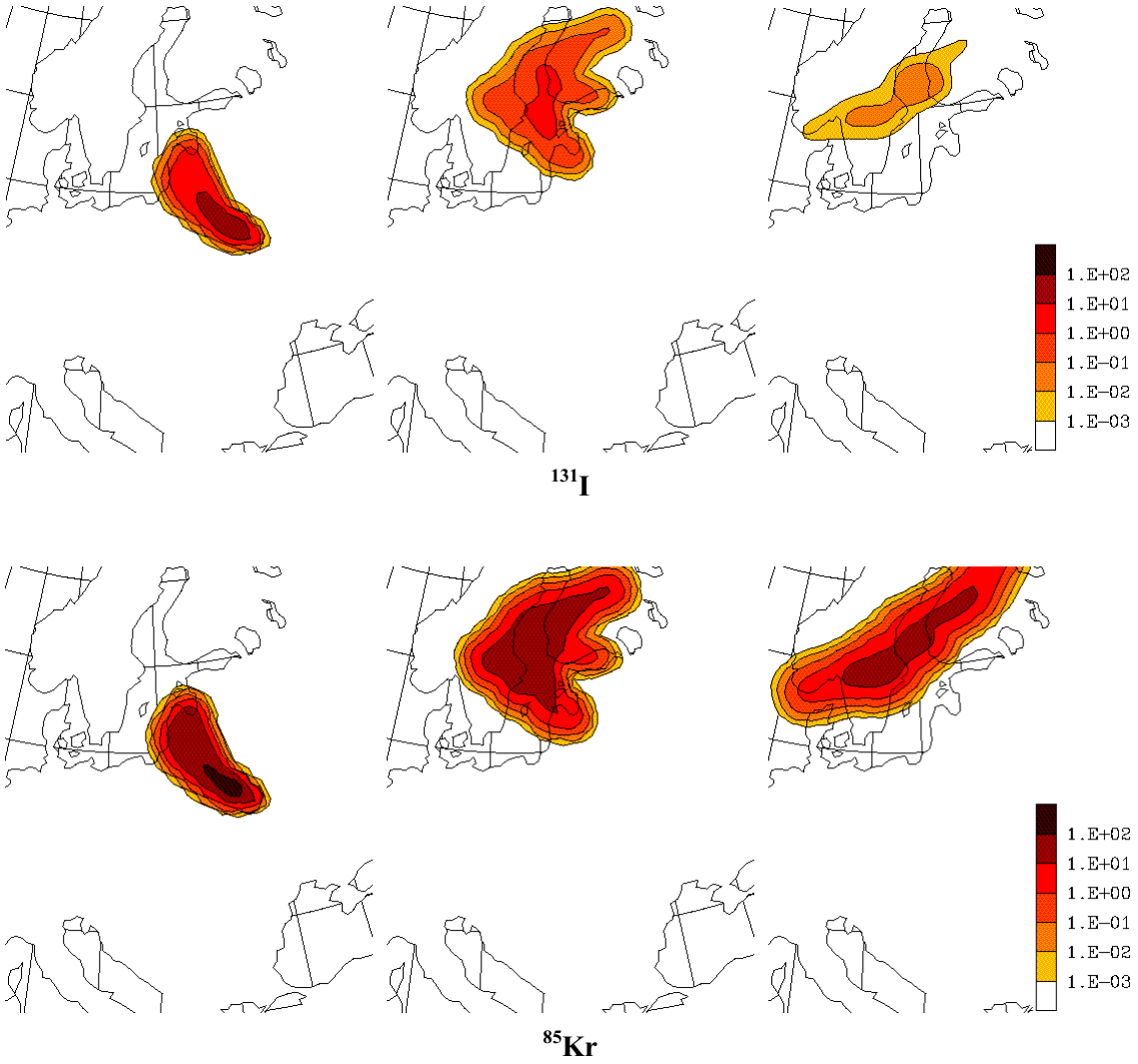

Figure 3.6.8. Radionuclide (top plate – ^{137}Cs; middle plate - ^{131}I; bottom plate - ^{85}Kr) air concentration fields at 00 UTC of 12 Apr 2002 (left), 13 Apr 2002 (middle), and 14 Apr 2002 (right) for DUHR occurred during 24 hours (10-11 Apr 2002, 12 UTC) at the Chernobyl NPP.

The time integrated air concentrations of radionuclides at 14 Apr 2002, 00 UTC for the same release at the Chernobyl NPP are shown in Fig. 3.6.9. Because both ^{137}Cs and ^{131}I undergo the deposition processes the areas enclosed by the highest TIAC isoline (1e+2 Bq·h/m^3) will be significantly smaller compared with ^{85}Kr. The highest TIAC for ^{137}Cs will be less frequent over the populated territories of the Scandinavian Peninsula than for ^{85}Kr. Moreover, the TIAC of ^{131}I will be less by an order of magnitude compared with both ^{137}Cs and ^{85}Kr.

The total deposition fields (as a sum of dry and wet depositions) of radionuclides at 14 Apr 2002, 00 UTC for the same release at the Chernobyl NPP are shown in Fig. 3.6.10. Only deposition for two nuclides - ^{137}Cs and ^{131}I – was considered because for noble gases a deposition is not included. The area of the fields enclosed by the lowest isoline of 10^0 Bq/m^2 is larger for ^{137}Cs compared with ^{131}I due to significant differences in deposition velocities and life-times of these nuclides. The higher deposition levels, ranging from 1e+2 to 1e+4 Bq/m^2, are observed 1) in vicinity of the Chernobyl NPP following the north-western direction of atmospheric transport during the first day, and 2) over the populated territories of the Baltic States, Belarus, and Scandinavian Peninsula (Sweden and Finland).

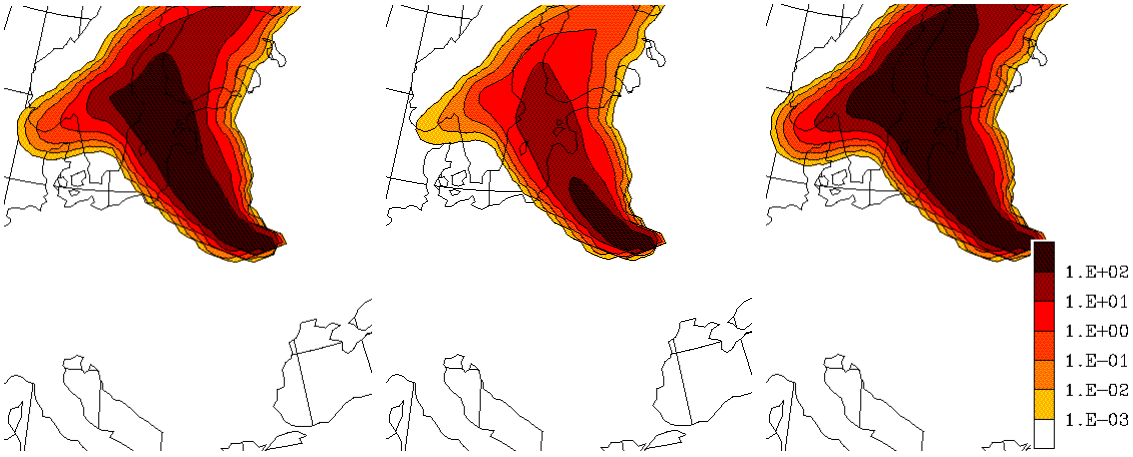

Figure 3.6.9. Time integrated air concentration fields of a) ^{137}Cs, b) ^{131}I, and c) ^{85}Kr at 14 Apr 2002, 00 UTC for DUHR occurred during 24 hours (10-11 Apr 2002, 12 UTC) at the Chernobyl NPP.

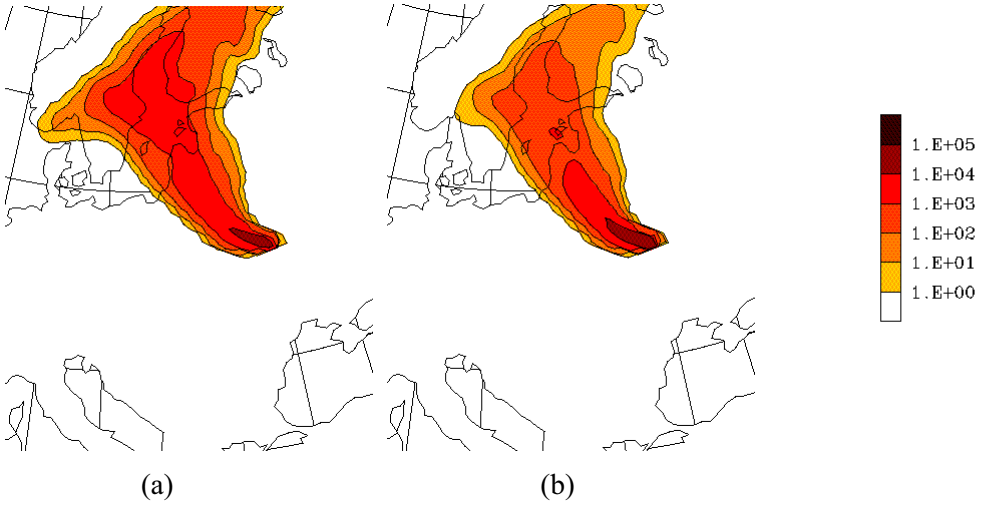

Figure 3.6.10. Total deposition fields of a) ^{137}Cs and b) ^{131}I at 14 Apr 2002, 00 UTC for DUHR occurred during 24 hours (10-11 Apr 2002, 12 UTC) at the Chernobyl NPP.

3.7. *ESTIMATION OF POTENTIAL IMPACT AT COPENHAGEN, DENMARK DUE TO RELEASES AT SELECTED NUCLEAR RISK SITES*

As an example, let us estimate a potential impact of the NRSs' hypothetical releases on one of the Nordic countries' capitals – Copenhagen, Denmark. The results of long-term modelling of atmospheric transport, dispersion, and deposition patterns represented by the TIAC, DD, and WD fields were used to evaluate the annual average levels concentration and depositions of ^{137}Cs and ranking of potential impact from selected in this study NRSs on the city. As shown in Tab. 3.7.1, four risk sites are located within a 500-km circle around Copenhagen: Barsebaeck, Ringhals, Oskarshamn NPPs of Sweden and the block of the German NPPs. For these sites, the estimated TIAC at Copenhagen varied between 1e+3–1e+2 Bq·h/m^3 and depositions are 1e+4-1e+2 Bq/m^2. The contribution of the wet deposition into the total deposition pattern varies between 46 and 76%.

Table 3.7.1. Annual average ^{137}Cs time integrated air concentration, dry, wet, and total depositions, and percentage contribution of wet deposition at Copenhagen, Denmark resulted from the hypothetical release at selected risk sites.

Copenhagen, Denmark vs. NRS	Distance to city, km	TIAC, Bq·h/m^3	DD, Bq/m^2	WD, Bq/m^2	TD, Bq/m^2	WD/TD, %
BNP - Barsebaeck NPP, Sweden	**28**	1,92E+3	1,04E+4	1,68E+4	2,72E+4	**62**
RNP - Ringhals NPP, Sweden	**234**	1,95E+2	1,05E+3	8,82E+2	1,93E+3	46
ONP - Oskarshamn NPP, Sweden	**298**	1,73E+2	9,32E+2	1,59E+3	2,53E+3	**63**
BGP - German NPPs, Germany	**334**	1,16E+2	6,27E+2	1,97E+3	2,60E+3	**76**
FNP - Forshmark NPP, Sweden	**623**	4,34E+1	2,35E+2	1,68E+2	4,03E+2	42
TRS - Olkiluoto NPP, Finland	**828**	2,42E+1	1,31E+2	2,50E+2	3,80E+2	**66**
INP - Ignalina NPP, Lithuania	**842**	2,33E+1	1,26E+2	2,34E+2	3,60E+2	**65**
LRS - Loviisa NPP, Finland	**976**	2,54E+1	1,37E+2	2,98E+2	4,35E+2	**68**
BBP - British NPPs, UK	1029	2,35E+1	1,27E+2	3,40E+2	4,67E+2	**73**
LNP - Leningrad NPP, Russia	1077	1,50E+1	8,10E+1	7,68E+1	1,58E+2	49
SNP - Smolensk NPP, Russia	1231	5,10E+0	2,76E+1	4,20E+1	6,96E+1	**60**
CNP - Chernobyl NPP, Ukraine	1261	7,34E+0	3,96E+1	9,70E+1	1,37E+2	**71**
KNP - Kola NPP, Russia	1697	3,58E-1	1,93E+0	1,00E+0	2,93E+0	34
KNS - Kola NS, Russia	1827	3,08E-1	1,69E+0	8,27E-1	2,52E+0	33
NZS - Novaya Zemlya, Russia	2665	1,51E-3	8,14E-3	3,56E-2	4,37E-2	**81**

Another four NRSs – Forshmark, Olkiluoto, Ignalina, and Loviisa NPPs – are situated within a 1000-km circle. For these risk sites, the estimated TIACs are within the first order of magnitude, and depositions are within the second order of magnitude. For all sites, except Forshmark, the wet deposition contributes more than 65% into the total deposition. Moreover, the total deposition at Copenhagen resulted from a hypothetical release at the Loviisa NPP is higher (4.35e+2 Bq/m^2) compared with the Ignalina and Olkiluoto NPPs, although the distance to the Danish capital is shorter for two later sites.

All other sites, except those of the Arctic latitudes – i.e. on the Kola Peninsula and Novaya Zemlya, are located within a 1500-km circle around Copenhagen. For these sites the concentration at city varies between 1e+3-1e+2 Bq·h/m^3 and depositions are 1e+4-1e+2 Bq/m^2. For the Arctic sites, TIACs are between 1e-1-1e-3 Bq·h/m^3 and depositions are 1e+0-1e-2 Bq/m^2. The contribution of wet deposition is more than two times higher for the Novaya Zemlya site (NZS) compared with the Kola Peninsula sites (KNP and KNS).

The ranking of the NRS impact (from potential maximum impact to potential minimum impact) at Copenhagen based on distance from the city to NRSs, and patterns of ^{137}Cs for TIAC, DD, WD, and TD is shown in Tab. 3.7.2. For each site the values of these patterns are given too. Although the impact decreases with the increasing of the distance from the city, it is not always a case: impact became less pronounced after the first 500 kilometres, i.e. it became evident during transformation from the meso- to large scales. The ranks of NRSs are also shifted and changed when additionally a wet deposition is accounted; although for the time integrated air concentration and dry deposition this ranking is identical. Such changes reflect dependence of impact on several key factors such as distance, dominating flow, precipitation patterns. Although the TRS, INP, LRS, and FNP sites are located closer (distance) to Copenhagen, the BBP site represents the higher level of potential impact compared with the later sites when the wet deposition is also taken into account.

Table 3.7.2. Ranking of potential impact at Copenhagen, Denmark resulted from the hypothetical releases at selected NRSs as a function of distance, annual average ^{137}Cs time integrated air concentration, dry, wet, and total depositions.

Ranking of NRS potential impact based on estimated **distance** (min -> max)															
Range	***1***	***2***	***3***	***4***	***5***	***6***	***7***	***8***	***9***	***10***	***11***	***12***	***13***	***14***	***15***
NRS	BNP	RNP	ONP	BGP	FNP	TRS	INP	LRS	BBP	LNP	SNP	CNP	KNP	KNS	NZS
km	28	234	298	334	623	828	842	976	1029	1077	1231	1261	1697	1827	2665
Ranking of NRS potential impact based on estimated **time integrated air concentration, TIAC** (max -> min)															
NRS	BNP	RNP	ONP	BGP	FNP	LRS	TRS	BBP	INP	LNP	CNP	SNP	KNP	KRS	NZS
Ranking of NRS potential impact based on estimated **dry deposition, DD** (max -> min)															
NRS	BNP	RNP	ONP	BGP	FNP	LRS	TRS	BBP	INP	LNP	CNP	SNP	KNP	KRS	NZS
Ranking of NRS potential impact based on estimated **wet deposition, WD** (max -> min)															
NRS	BNP	BGP	ONP	RNP	BBP	LRS	TRS	INP	FNP	CNP	LNP	SNP	KNP	KRS	NZS
Ranking of NRS potential impact based on estimated **total deposition, TD** (max -> min)															
NRS	BNP	BGP	ONP	RNP	BBP	LRS	FNP	TRS	INP	LNP	CNP	SNP	KNP	KRS	NZS

Table 3.7.3. Ranking of potential impact at Copenhagen, Denmark resulted from the hypothetical releases at selected NRSs as a function of typical transport time, maximum reaching distance, maximum possible impact zone, and fast transport probability fields.

Ranking of NRS potential impact based on **typical transport time, TTT** (in days, min->max)											
NRS	BBP	BGP	BNP	ONP	RNP	LRS	TRS	INP	LNP	KNP	NZS
TTT	**1.5**	**0.5**	**0.1**	**0.6**	**0.4**	**2.3**	**2.4**	**1.4**	**2.4**	>2.5	>2.5
Ranking of NRS potential impact based on 1 day **maximum reaching distance, MRD** (yes + or no -)											
NRS	BBP	BGP	BNP	ONP	RNP	LRS	TRS	INP	LNP	KNP	NZS
MRD	+	+	+	+	+	+	+	+	-	-	-
Ranking of NRS potential impact based on 1 day **maximum possible impact zone, MPIZ** (yes + or no -)											
NRS	BBP	BGP	BNP	ONP	RNP	LRS	TRS	INP	LNP	KNP	NZS
MPIZ	-	-	+	-	+	-	-	-	-	-	-
Ranking of NRS potential impact based on **fast transport probability fields, FTPF** (% of AHPPI)											
NRS	BBP	BGP	BNP	ONP	RNP	LRS	TRS	INP	LNP	KNP	NZS
FTPF, 12h	<20	**80**	**100**	**45**	**80**	<20	<20	<20	<20	<20	<20
FTPF, 24h	**55**	**95**	**95**	**70**	**80**	<20	<20	<20	<20	<20	<20

For comparative purposes the ranking of potential impact at Copenhagen is also given on a base of the probabilistic analyses of atmospheric trajectories calculated for a multiyear period for 11 NRSs (*Mahura & Baklanov, 2002*). The summarized output is shown in Tab. 3.7.3. The typical transport time, TTT (measured in days of atmospheric transport); maximum reaching distance, MRD (represents a possibility of event that at least one trajectory arrived at city); maximum possible impact zone, MPIZ (underlines a possibility of the highest impact from the site to the city);

and fast transport probability fields (shows a scale of potential impact due to atmospheric transport with respect to the area where such impact can be the highest). The MPIZ indicator showed that only two risk sites represented the highest risk for Copenhagen. Although from all others sites, except the Arctic sites and Leningrad NPP, there is a potential possibility of contaminated air mass arrival at city (as showed the MRD indicator). Typically the atmospheric transport from the BGP, BNP, ONP, and RNP sites to Copenhagen can occur in less than 1 day. Because we had limited construction of the TTT fields by 2.5 days, for the Arctic latitude sites it is undefined (>2.5). The fast transport probability fields for both terms of 12 and 24 hours showed dominance of impact from the same risk sites.

Finally, it should be noted that combination of both analyses, using results of the probabilistic long-term trajectory and dispersion modelling (which were two interrelated parts of the AR-NARP project methodological developments and testing applicability) from the selected sites, will provide more detailed level, quality, and accuracy in evaluation of potential impact on both geographical particular location (city, site, etc.) and region (country, county, etc.). It should be reminded that in this study we did not consider probabilities and severities of possible accidents from different types of nuclear risk sites, and only geophysical factors of atmospheric transport and deposition were considered.

CONCLUSIONS

The main aim of this study was to combine atmospheric transport and dispersion modelling and statistical analyses to assess consequences of an accidental release at the selected nuclear risk sites (NRS) located in the Euro-Arctic region. The main purpose of this study was a probabilistic analysis of atmospheric transport and deposition patterns from these sites for the GIS-based studies of vulnerability to radioactive deposition and risk assessment of impact.

The nuclear risk sites of concern selected in this study are 16 sites including nuclear power plants, nuclear submarine bases, nuclear processing plant, and former nuclear weapons testing site. The countries and geographical regions of interest are the Nordic countries, Baltic States, Eastern and Western European countries of the Northern Europe, Belarus, Ukraine, and the European territories of the Russian Federation.

Once the risk sites and geographical regions of interest are defined, it is of particular interest to answer the following questions: *Which geographical territories are at highest risk from accidental releases at NRSs? What are probabilities for radionuclide atmospheric transport and deposition on neighbouring countries in case of accidents at NRSs*?

To answer these questions we employed the methodology developed within the "Arctic Risk" NARP Project (*AR-NARP, 2001-2003; Baklanov et al., 2002b*) and based on the long-term probabilistic dispersion modelling approach. The first research tool was the DERMA model to simulate 5-day atmospheric transport, dispersion, and deposition of ^{137}Cs for a one-day release (at rate of 10^{11} Bq/s). As input data we used the DMI-HIRLAM and ECMWF meteorological gridded fields. The second research tool was a set of statistical methods (including exploratory and probability fields analyses) for analysis of dispersion modelling results. Additionally, several specific dates when atmospheric transport occurred towards the geographical regions of interest were also evaluated for selected NRSs.

The results of probabilistic analysis of dispersion modelling results for NRSs are presented as a set of various indicators of the NRS possible impact on the geographical regions of interest. In this study, we calculated, constructed, and evaluated several indicators based on dispersion modelling results: time integrated air concentration (TIAC) at the ground surface, dry deposition (DD), and

wet deposition (WD) patterns. To evaluate the temporal variability of these indicators, analyses were performed on an annual, seasonal, and monthly basis.

Based on analysis of dispersion modelling results the general findings are the following.

For the long-term simulation, the time integrated air concentration and dry deposition have higher values in vicinity of the sites, and they decrease by 1-2 orders of magnitude for approximately every 1000 km. Moreover, both types of fields have an elliptical form. The shape of these fields, in some way, reflects the dominating airflow patterns from the sites throughout the year. For most of the sites these fields showed the prevailing atmospheric transport by westerly flows. Although wet deposition is also high near the sites, the WD field can have several local maxima remotely situated from the sites, this field is less smooth, and this field has a cellular structure strongly depending on irregularity of the rainfall patterns. Among 16 risk sites considered in this study several groups can be identified based on temporal and spatial distribution of TIAC, DD, and WD fields. These groups consisted of the sites located in the maritime area, inland area, Arctic latitudes area, and intermediate area between the maritime and continental types of the climate regimes.

Analysis of specific cases showed several common peculiarities. First, shapes and magnitude of isolines are almost similar for both ^{137}Cs and ^{90}Sr TIAC and DD fields, and both fields are well correlated. Second, ^{131}I TIAC decreases faster with a distance from the site compared with ^{137}Cs and ^{90}Sr due to radioactive decay and greater possibility to serve as condensation nuclei. Third, the WD fields showed a similar structural irregularity of fields (as seasonal and monthly variability) compared with the TIAC and DD fields.

The ranking of potential impact at Copenhagen from the selected NRSs showed that although for the time integrated air concentration and dry deposition the order of such ranking is identical, when additionally a wet deposition is accounted the order of ranking can change significantly already on mesoscales. Due to a relative proximity (≤ 500 km) to Copenhagen, the block of the German NPPs, Barsebaeck, Oskarshamn, and Ringhals NPPs represent the first four risk sites of major concern for the city. Although several other sites such as the Olkiluoto, Ignalina, Loviisa, and Forshmark plants are located geographically closer to the city, the block of the British NPPs (1000 km) represents the higher risk of potential impact on Copenhagen compared with them.

The results of this study are applicable for: (i) better understanding of general atmospheric transport patterns in the event of an accidental release at NRSs, (ii) improvement of planning in emergency response to radionuclide releases from the NRS locations, (iii) studies of social and economical consequences of the NRS impact for population and environment of the neighbouring countries, (iv) multidisciplinary risk evaluation and vulnerability analysis, and (v) probabilistic assessment of radionuclide meso-, regional-, and long-range transport patterns; (vi) evaluation of integrated impact from the long-term releases/ emissions (such as, for example, the Sellafield processing plant).

The annual, seasonal, and monthly variability of the time integrated air concentration, dry, and wet deposition fields are stored on CD (enclosed with this report with enlarged figures, if ordered).

RECOMMENDATIONS FOR FUTURE STUDIES

Several concluding remarks and recommendations should be made to clarify applicability and importance of the obtained results. These results constitute initial steps to estimate atmospheric transport and deposition from selected nuclear risk sites. In the event of an accidental release these results can be used as a preliminary estimation of likelihood and direction of the atmospheric

transport, evaluation of minimum and average transport times, and identification of predominant atmospheric layer during transport reaching the borders of counties, countries, and remote geographical regions. They also can be used to estimate possible order of magnitudes for time integrated air concentration, and dry and wet deposition patterns of radionuclides at exact geographical locations or territories of concern. Using calculated concentration and deposition fields it is possible to evaluate doses due to inhalation and from the underlying contaminated surfaces accumulated or averaged over the year, season, or month.

Emergency response plans to possible radionuclide releases from the nuclear risk sites could be improved by analyses of probabilities for the fast transport, airflow patterns, typical transport time, maximum reaching distance and maximum possible impact zone indicators. Valuable indicators of the NRS possible impacts will be given by the temporal variability of the radionuclide time-integrated concentration, dry, wet, and total deposition patterns at various distances from the sites. These are input to better understanding of seriousness of possible consequences of radionuclide releases from the nuclear risk sites. This study output is valuable input data for studies of the health effects, social, and economical consequences for population and environment of the neighbouring countries, and especially, on a regional scale due to impact of accidents at NRSs. These results are also important data for studies of multidisciplinary risk and vulnerability, and probabilistic assessments of the radionuclide meso-, regional-, and long-range transport.

Moreover, we suggest that the developed methodology within the Arctic Risk NARP Project (*AR-NARP, 2001-2003*) and used in this study might be successfully applied for other sites of concern such as chemical, biological, and natural hazard, for assessments of the long-term impacts from existing emission/ release sources of different kinds of pollutants as well as for environmental problems of wider spectra.

Therefore, we recommend further studies on the following issues.

First, the analysis of the atmospheric transport and deposition patterns for selected NRSs raises a concern of the possible rapid transport as well as radionuclide deposition in the neighbouring to NRSs countries. Therefore, as a logical step to finalize this study we propose to evaluate: i) risks, socio-economical and geographical consequences for different geographical areas and population groups applying available demographic databases and GIS-technology, and ii) vulnerability to a radioactive deposition with a focus on the transfer of certain radionuclides into food-chains, especially for the native population, and considering risks for different geographical areas. Such analysis can provide a complete estimate of nuclear risk and regional vulnerability for geographical territories, countries, counties, and population groups in the Euro-Arctic region due to possible accidental releases at these NRSs.

Second, it should be mentioned that there are other nuclear risk sites in the European region, including more than 200 nuclear power plants, nuclear weapons-related facilities, nuclear fuel reprocessing facilities, spent nuclear fuel facilities, etc. An approach similar to used in this study could be applied for these sites too; and hence, a potential proposal could be written and submitted. In addition, because there is a high monthly variability in the airflow and deposition patterns from the sites to the regions of interest, we suggest investigating possible impacts of the NRS accidental releases using the source (nuclear risk site) vs. receptor (remote geographical location or region) relationship approach. For this purpose, the additional sensitivity of source vs. receptor indicators might be introduced by inverse modelling.

Third, there is a large number of potential risk sources located in the European region countries. These sources represent risks of different magnitude, and their danger is highly dependent on many factors. In general, the simplest approach depends on the knowledge of the

source term. But it seems reasonable to ask: What is the ranging of each radiation risk source with respect to another source as well as due to other factors? As a first step, an evaluation of the probability matrix for the transport patterns in different environments, rapid transport, and removal processes might give an answer to this question. For comprehensive evaluation, the additional factors such as probabilities of the accidental releases, prevailing scenarios, accumulated activities, types of radioactive material, etc. should be considered too. Such analysis might rank the risk sources in the order of their potential danger with respect to population and environment of different territories. This allows the policy and decision makers to make an informed decision about: which sources should be considered as the first priority of study, and what measures should be taken if an accidental release will occur. Of course, for an accident, the detailed examination of the conditions at the site, the accident scenario and actual atmospheric conditions must be taken into account.

ACKNOWLEDGMENTS

The authors are grateful to Drs. Leif Laursen (Danish Meteorological Institute), Boris Segerståhl (Thule Institute, University of Oulu, Finland), Ronny Bergman (Swedish Defence Research Authority), Morten Sickkel (Norwegian Radiation Protection Authority), Olga Rigina (Danish Technical University), Sergey Morozov (Institute of Northern Environmental Problems, Kola Science Center, Russia), Sven Nielsen (Risø National Laboratory, Denmark), Vladislav Golikov (Institute of Radiation Hygiene, St. Petersburg, Russia), Torben Mikkelsen (Risø National Laboratory, Denmark), Steen C. Hoe (Danish Emergency Management Agency) for collaboration, discussions and constructive comments.

The computer facilities at the Danish Meteorological Institute (DMI) have been used extensively in the study. The DMI-HIRLAM and ECMWF meteorological data were used as input data for the dispersion modelling. The authors are grateful to the DMI Computer Support, HIRLAM group and Data Processing Department for the collaboration, computer assistance, and advice.

Financial support of this study included the grants of the Nordic Arctic Research Programme (NARP) and Nordisk Forskerutdanningsakademi (NorFA).

REFERENCES

Amosov, P.V., A.A. Baklanov, S.I. Mazukhina (**1995**) Estimation of potential risk for the population from the hypothetical accident at the Kola nuclear power plant. In: *The 2nd International Conference on Environmental radioactivity in the Arctic*. Oslo, August 21-25, 1995, pp. 365-368.

Andreev, I., Hittenberger, M., Hofer, P., Kromp-Kolb, H., Kromp, W., Seibert, P., Wotawa, G. (**1998**) Risks due to severe accidents of nuclear power plants in Europe - the methodology of riskmap. *J. Hazardous Materials*, 61, 257-262.

Andreev, I., Gazso, A., Gohla, H., Hofer, P., Kromp, W., Kromp-Kolb, H., Rehm, W., Seibert, P. (**2000**) Risks due to severe accidents of nuclear power plants in Europe - the methodology of RISKMAP – Possible extensions. In: *ESEE 2000: 3rd Int. Conference of the European Society for Ecological Economics*.

AR-NARP (**2001-2003**) On-going Project ´Atmospheric Transport Pathways, Vulnerability and Possible Accidental Consequences from the Nuclear Risk Sites in the European Arctic (*Arctic Risk*`)` of the NARP: Nordic Arctic Research Programme. *DMI* project web site: http://www.dmi.dk/f+u/luft/eng/arctic-risk/main.html.

Baklanov, A.A., A.G. Mahura, S.V. Morozov (**1994**) The Simulation of Radioactive Pollution of the Environment After an Hypothetical Accident at the Kola Nuclear Power Plant*. J. Environmental Radioactivity,* 25, 65-84.

Baklanov, A. **(2000**) Modelling of episodes of atmospheric transport and deposition: Hypothetical nuclear accidents in North-West Russia. In: *Nuclear Risks, Environmental and Development Cooperation in the North of Europe*. CERUM, University of Umea, Sweden, pp. 57-72.

Baklanov A., Mahura A. (**2001**) Atmospheric Transport Pathways, Vulnerability and Possible Accidental Consequences from the Nuclear Risk Sites: Methodology for Probabilistic Atmospheric Studies*. DMI Sci. Report* #01-9. ISBN: 87-7478-450-1, 43 p.

Baklanov A., Sørensen J.H., (**2001**) Parameterisation of radionuclide deposition in atmospheric dispersion models. *Phys. Chem. Earth, (B)*, 26, 787–799.

Baklanov A., R. Bergman, C. Lundström, L. Thaning (**2001**) Modelling of episodes of atmospheric transport and deposition from hypothetical nuclear accidents on the Kola peninsula. *CERUM Northern Studies Working Paper No. 23*. Umeå university, Sweden.

Baklanov, A. (**2002**) Methodologies for multidisciplinary nuclear risk and vulnerability assessments in the Arctic and Sub-Arctic. *NATO Science Series, Kluwer Academic Publishers*, (in press)

Baklanov, A., A. Mahura, D. Jaffe, L. Thaning, R.Bergman, R.Andres (**2002a**) Atmospheric Transport Patterns and Possible Consequences for the European North after a Nuclear Accident. *Journal of Environmental Radioactivity,* 60, 23-48.

Baklanov, A., A. Mahura, J.H. Sørensen, O. Rigina, R. Bergman (**2002b**) Methodology for Risk Analysis based on Atmospheric Dispersion Modelling from Nuclear Risk Sites. *Danish Meteorological Institute, Scientific Report*, 02-16, ISBN: 87-7478-470-6, 54 p.

Baklanov, A., A. Mahura, J.H. Sørensen (**2003**) Methodology for Prediction and Estimation of Consequences of Possible Atmospheric Releases of Hazardous Matter: 'Kursk' Submarine Study. *Atmospheric Chemistry and Physics*, Vol 3, 1-42.

Bergman, R., Ulvsand, T. (**1994**). Intervention in regular practice to bring down external exposure to agricultural personnel or activity transfer over certain boreal food-chains. *FOA report*, National Defence Research Establishment, Dept of NBC Defence, S-90182 Umeå, Sweden.

Bergman, R., Thaning, L., Baklanov, A. (**1998**) Site-sensitive hazards of potential airborne radioactive release from sources on the Kola Peninsula. *FOA report*: FOA-R—00717-861--SE, February 1998, 14 p.

Dahlgaard, H., Editor (**1994**) Nordic Radioecology: The transfer of radionuclides through Nordic ecosystems to man. Amsterdam, Elsevier Science B. V. *Studies in Environmental Science* 62.

IIASA (**1996**) Baklanov A., Bergman R., Segerståhl B. Radioactive sources in the Kola region: Actual and potential radiological consequences for man. *Report, International Institute for Applied Systems Analysis. Laxenburg*, Austria, IIASA, Radiation Safety of the Biosphere, 255 p.

Mahura, A.G., Jaffe, D., Andres, R., Merrill, J. (**1999**) Atmospheric transport pathways from the Bilibino nuclear power plant to Alaska. *Atmospheric Environment*, 33/30, 5115-5122.

Mahura A., Baklanov A., (**2002**) Probabilistic Analysis of Atmospheric Transport Patterns from Nuclear Risk Sites in Euro-Arctic Region. *Danish Meteorological Institute, Scientific Report*, 02-15, ISBN: 87-7478-469-2, 87p.

Moberg, L., Editor (**1991**) *The Chernobyl fallout in Sweden. Results from a research programme on environmental radiology*. The Swedish Radiation Protection Institute, Stockholm, Sweden.

NATO (**1998**): Cross-Border Environmental Problems Emanating from Defence-Related Installations and Activitis. *NATO/CCMS Pilot Study, Phase II: 1995-1998, Final Report*, Vol 4, March 1998, p. I-81-84.

Rantalainen, L. (**1995**) Source terms of the Kola nuclear power plant and risk of severe environmental contamination. In: *The 2nd International Conference on Environmental radioactivity in the Arctic*. Oslo, August 21-25, 1995.

Saltbones J., A.Foss, J.Bartnicki (**2000**) Threat to Norway from potential accidents at the Kola nuclear power plant. Climatological trajectory analysis and episode studies. *Atmospheric Environment*, 34(3), 407-41

Sinyak, Y. (**1995**) Nuclear Energy in Eastern Europe and the Former Soviet Union: How Safe and How Much?, *International Institute for Applied Systems Analysis (IIASA) Sci. Report*, Sum 1995.

Slaper, H., Eggink, G.J., Blaauboer, R.O. (**1994**) Risk assessment method for accidental releases from nuclear power plants in Europe. *Report of the National Institute of public health and the environment*. Bilthoven, Netherlands.

Smith, F. (**1998**) Estimating the Statistics of Risk from a Hazardous Source at Long Range, *Atmospheric Environment*, 32(16): 2775-2791.

Sørensen, J.H. (**1998**) Sensitivity of the DERMA Long-Range Gaussian Dispersion Model to Meteorological Input and Diffusion Parameters. *Atmos. Environ*. 32, 4195-4206.

Sørensen, J.H., A. Rasmussen, T. Ellermann, E. Lyck (**1998**) Mesoscale Influence on Long-range Transport; Evidence from ETEX Modelling and Observations, *Atmospheric Environment,* 32, 4207-4217.

Thaning, L., Baklanov, A. (**1997**) Simulation of atmospheric transport and deposition on the local/meso- and regional scales after hypothetical accidents at Kola Nuclear Power Plant. *Scien. Tot. Envir.*, 202, 199-210.

ABBREVIATIONS

AR-NARP	"Arctic Risk" Project - Nordic Arctic Research Programme
BBP	Block of the British NPPs
BGP	Block of the German NPPs
BNP	Barsebaeck Nuclear Power Plant
CNP	Chernobyl Nuclear Power Plant
DD	Dry Deposition
DERMA	Danish Emergency Response Model for Atmosphere
DMI	Danish Meteorological Institute
ECMWF	European Center for Medium Weather Forecast
FNP	Forsmark Nuclear Power Plant
GIS	Geographic Information System
HIRLAM	HIgh Resolution Limited Area Model
INP	Ignalina Nuclear Power Plant
KNP	Kola Nuclear Power Plant
KNS	Kola (Roslyakovo Shipyard) Nuclear Risk Site
KRS	Kursk Nuclear Power Plant
LNP	Leningrad Nuclear Power Plant
LRS	Loviisa Nuclear Power Plant
NPP	Nuclear Power Plant
NRS	Nuclear Risk Site
NZS	Novaya Zemlya Test Site
ONP	Oskarshamn Nuclear Power Plant
RNP	Ringhals Nuclear Power Plant
SNP	Smolensk Nuclear Power Plant
TD	Total Deposition
TIAC	Time Integrated Air Concentration
TRS	Olkiluoto (TVO) Nuclear Power Plant
UDHR	Unit Discrete Hypothetical Release
WD	Wet Deposition

DANISH METEOROLOGICAL INSTITUTE

Scientific Reports

Scientific reports from the Danish Meteorological Institute cover a variety of geophysical fields, i.e. meteorology (including climatology), oceanography, subjects on air and sea pollution, geomagnetism, solar-terrestrial physics, and physics of the middle and upper atmosphere.

Reports in the series within the last five years:

No. 99-1
Henrik Feddersen: Project on prediction of climate variations on seasonel to interannual timescales (PROVOST) EU contract ENVA4-CT95-0109: DMI contribution to the final report: Statistical analysis and post-processing of uncoupled PROVOST simulations

No. 99-2
Wilhelm May: A time-slice experiment with the ECHAM4 A-GCM at high resolution: the experimental design and the assessment of climate change as compared to a greenhouse gas experiment with ECHAM4/OPYC at low resolution

No. 99-3
Niels Larsen et al.: European stratospheric monitoring stations in the Artic II: CEC Environment and Climate Programme Contract ENV4-CT95-0136. DMI Contributions to the project

No. 99-4
Alexander Baklanov: Parameterisation of the deposition processes and radioactive decay: a review and some preliminary results with the DERMA model

No. 99-5
Mette Dahl Mortensen: Non-linear high resolution inversion of radio occultation data

No. 99-6
Stig Syndergaard: Retrieval analysis and methodologies in atmospheric limb sounding using the GNSS radio occultation technique

No. 99-7
Jun She, Jacob Woge Nielsen: Operational wave forecasts over the Baltic and North Sea

No. 99-8
Henrik Feddersen: Monthly temperature forecasts for Denmark - statistical or dynamical?

No. 99-9
P. Thejll, K. Lassen: Solar forcing of the Northern hemisphere air temperature: new data

No. 99-10
Torben Stockflet Jørgensen, Aksel Walløe Hansen: Comment on "Variation of cosmic ray flux and global coverage - a missing link in solar-climate relationships" by Henrik Svensmark and Eigil Friis-Christensen

No. 99-11
Mette Dahl Meincke: Inversion methods for atmospheric profiling with GPS occultations

No. 99-12
Hans-Henrik Benzon; Laust Olsen; Per Høeg: Simulations of current density measurements with a Faraday Current Meter and a magnetometer

No. 00-01
Per Høeg; G. Leppelmeier: ACE - Atmosphere Climate Experiment

No. 00-02
Per Høeg: FACE-IT: Field-Aligned Current Experiment in the Ionosphere and Thermosphere

No. 00-03
Allan Gross: Surface ozone and tropospheric chemistry with applications to regional air quality modeling. PhD thesis

No. 00-04
Henrik Vedel: Conversion of WGS84 geometric heights to NWP model HIRLAM geopotential heights

No. 00-05
Jérôme Chenevez: Advection experiments with DMI-Hirlam-Tracer

No. 00-06
Niels Larsen: Polar stratospheric clouds micro-physical and optical models

No. 00-07
Alix Rasmussen: "Uncertainty of meteorological parameters from DMI-HIRLAM"

No. 00-08
A.L. Morozova: Solar activity and Earth's weather. Effect of the forced atmospheric transparency changes on the troposphere temperature profile studied with atmospheric models

No. 00-09
Niels Larsen, Bjørn M. Knudsen, Michael Gauss, Giovanni Pitari: Effects from high-speed civil traffic aircraft emissions on polar stratospheric clouds

No. 00-10
Søren Andersen: Evaluation of SSM/I sea ice algorithms for use in the SAF on ocean and sea ice, July 2000

No. 00-11
Claus Petersen, Niels Woetmann Nielsen: Diagnosis of visibility in DMI-HIRLAM

No. 00-12
Erik Buch: A monograph on the physical oceanography of the Greenland waters

No. 00-13
M. Steffensen: Stability indices as indicators of lightning and thunder

No. 00-14
Bjarne Amstrup, Kristian S. Mogensen, Xiang-Yu Huang: Use of GPS observations in an optimum interpolation based data assimilation system

No. 00-15
Mads Hvid Nielsen: Dynamisk beskrivelse og hydrografisk klassifikation af den jyske kyststrøm

No. 00-16
Kristian S. Mogensen, Jess U. Jørgensen, Bjarne Amstrup, Xiaohua Yang and Xiang-Yu Huang: Towards an operational implementation of HIRLAM 3D-VAR at DMI

No. 00-17
Sattler, Kai; Huang, Xiang-Yu: Structure function characteristics for 2 meter temperature and relative humidity in different horizontal resolutions

No. 00-18
Niels Larsen, Ib Steen Mikkelsen, Bjørn M. Knudsen m.fl.: In-situ analysis of aerosols and gases in the polar stratosphere. A contribution to THESEO. Environment and climate research programme. Contract no. ENV4-CT97-0523. Final report

No. 00-19
Amstrup, Bjarne: EUCOS observing system experiments with the DMI HIRLAM optimum interpolation analysis and forecasting system

No. 01-01
V.O. Papitashvili, L.I. Gromova, V.A. Popov and O. Rasmussen: Northern polar cap magnetic activity index PCN: Effective area, universal time, seasonal, and solar cycle variations

No. 01-02
M.E. Gorbunov: Radioholographic methods for processing radio occultation data in multipath regions

No. 01-03
Niels Woetmann Nielsen; Claus Petersen: Calculation of wind gusts in DMI-HIRLAM

No. 01-04
Vladimir Penenko; Alexander Baklanov: Methods of sensitivity theory and inverse modeling for estimation of source parameter and risk/vulnerability areas

No. 01-05
Sergej Zilitinkevich; Alexander Baklanov; Jutta Rost; Ann-Sofi Smedman, Vasiliy Lykosov and Pierluigi Calanca: Diagnostic and prognostic equations for the depth of the stably stratified Ekman boundary layer

No. 01-06
Bjarne Amstrup: Impact of ATOVS AMSU-A radiance data in the DMI-HIRLAM 3D-Var analysis and forecasting system

No. 01-07
Sergej Zilitinkevich; Alexander Baklanov: Calculation of the height of stable boundary layers in operational models

No. 01-08
Vibeke Huess: Sea level variations in the North Sea – from tide gauges, altimetry and modelling

No. 01-09
Alexander Baklanov and Alexander Mahura: Atmospheric transport pathways, vulnerability and possible accidental consequences from nuclear risk sites: methodology for probabilistic atmospheric studies

No. 02-01
Bent Hansen Sass and Claus Petersen: Short range atmospheric forecasts using a nudging procedure to combine analyses of cloud and precipitation with a numerical forecast model

No. 02-02
Erik Buch: Present oceanographic conditions in Greenland waters

No. 02-03
Bjørn M. Knudsen, Signe B. Andersen and Allan Gross: Contribution of the Danish Meteorological Institute to the final report of SAMMOA. CEC contract EVK2-1999-00315: Spring-to.-autumn measurements and modelling of ozone and active species

No. 02-04
Nicolai Kliem: Numerical ocean and sea ice modelling: the area around Cape Farewell (Ph.D. thesis)

No. 02-05
Niels Woetmann Nielsen: The structure and dynamics of the atmospheric boundary layer

No. 02-06
Arne Skov Jensen, Hans-Henrik Benzon and Martin S. Lohmann: A new high resolution method for processing radio occultation data

No. 02-07
Per Høeg and Gottfried Kirchengast: ACE+: Atmosphere and Climate Explorer

No. 02-08
Rashpal Gill: SAR surface cover classification using distribution matching

No. 02-09
Kai Sattler, Jun She, Bent Hansen Sass, Leif Laursen, Lars Landberg, Morten Nielsen og Henning S. Christensen: Enhanced description of the wind climate in Denmark for determination of wind resources: final report for 1363/00-0020: Supported by the Danish Energy Authority

No. 02-10
Michael E. Gorbunov and Kent B. Lauritsen: Canonical transform methods for radio occultation data

No. 02-11
Kent B. Lauritsen and Martin S. Lohmann: Unfolding of radio occultation multipath behavior using phase models

No. 02-12
Rashpal Gill: SAR ice classification using fuzzy screening method

No. 02-13
Kai Sattler: Precipitation hindcasts of historical flood events

No. 02-14
Tina Christensen: Energetic electron precipitation studied by atmospheric x-rays

No. 02-15
Alexander Mahura and Alexander Baklanov: Probablistic analysis of atmospheric transport patterns from nuclear risk sites in Euro-Arctic Region

No. 02-16
A. Baklanov, A. Mahura, J.H. Sørensen, O. Rigina, R. Bergman: Methodology for risk analysis based on atmospheric dispersion modelling from nuclear risk sites

No. 02-17
A. Mahura, A. Baklanov, J.H. Sørensen, F. Parker, F. Novikov K. Brown, K. Compton: Probabilistic analysis of atmospheric transport and deposition patterns from nuclear risk sites in russian far east

No. 03-01
Hans-Henrik Benzon, Alan Steen Nielsen, Laust Olsen: An atmospheric wave optics propagator, theory and applications

No. 03-02
A.S. Jensen, M.S. Lohmann, H.-H. Benzon and A.S. Nielsen: Geometrical optics phase matching of radio occultation signals

No. 03-03
Bjarne Amstrup, Niels Woetmann Nielsen and Bent Hansen Sass: DMI-HIRLAM parallel tests with upstream and centered difference advection of the moisture variables for a summer and winter period in 2002

No. 03-04
Alexander Mahura, Dan Jaffe and Joyce Harris: Identification of sources and long term trends for pollutants in the Arctic using isentropic trajectory analysis

No. 03-05
Jakob Grove-Rasmussen: Atmospheric Water Vapour Detection using Satellite GPS Profiling

No. 03-06
Bjarne Amstrup: Impact of NOAA16 and NOAA17 ATOVS AMSU-A radiance data in the DMI-HIRLAM 3D-VAR analysis and forecasting system - January and February 2003

No. 03-07
Kai Sattler and Henrik Feddersen: An European Flood Forecasting System EFFS. Treatment of uncertainties in the prediction of heavy rainfall using different ensemble approaches with DMI-HIRLAM

No. 03-08
Peter Thejll and Torben Schmith: Limitations on regression analysis due to serially correlated residuals: Application to climate reconstruction from proxies

No. 03-09
Peter Stauning, Hermann Lühr, Pascale Ultré-Guérard, John LaBrecque, Michael Purucker, Fritz Primdahl, John L. Jørgensen, Freddy Christiansen, Per Høeg, Kent B. Lauritsen: OIST-4 Proceedings. 4'th Oersted International Science Team Conference. Copenhagen 23-27 September 2002

No. 03-10
Niels Woetmann Nielsen: A note on the sea surface momentum roughness length.

No. 03-11
Niels Woetmann Nielsen: Quasigeostrophic interpretation of extratropical cyclogenesis

No. 03-12
Alexander Baklanov: FUMAPEX – project kick-off meeting and first progress report. Integrated systems for forecasting urban meteorology, air pollution and population exposure, EVK4-CT-2002-00097

No. 03-13
Rasmus Tonboe, Søren Andersen, Leif Toudal: Anomalous winter sea ice backscatter and brightness temperatures

No. 03-14
Alexander Mahura, Alexander Baklanov, Jens Havskov Sørensen: Long-term probabilistic atmospheric transport and deposition patterns from nuclear risk sites in euro-arctic region. Arctic risk – project of the Nordic Arctic Research Programme (NARP)